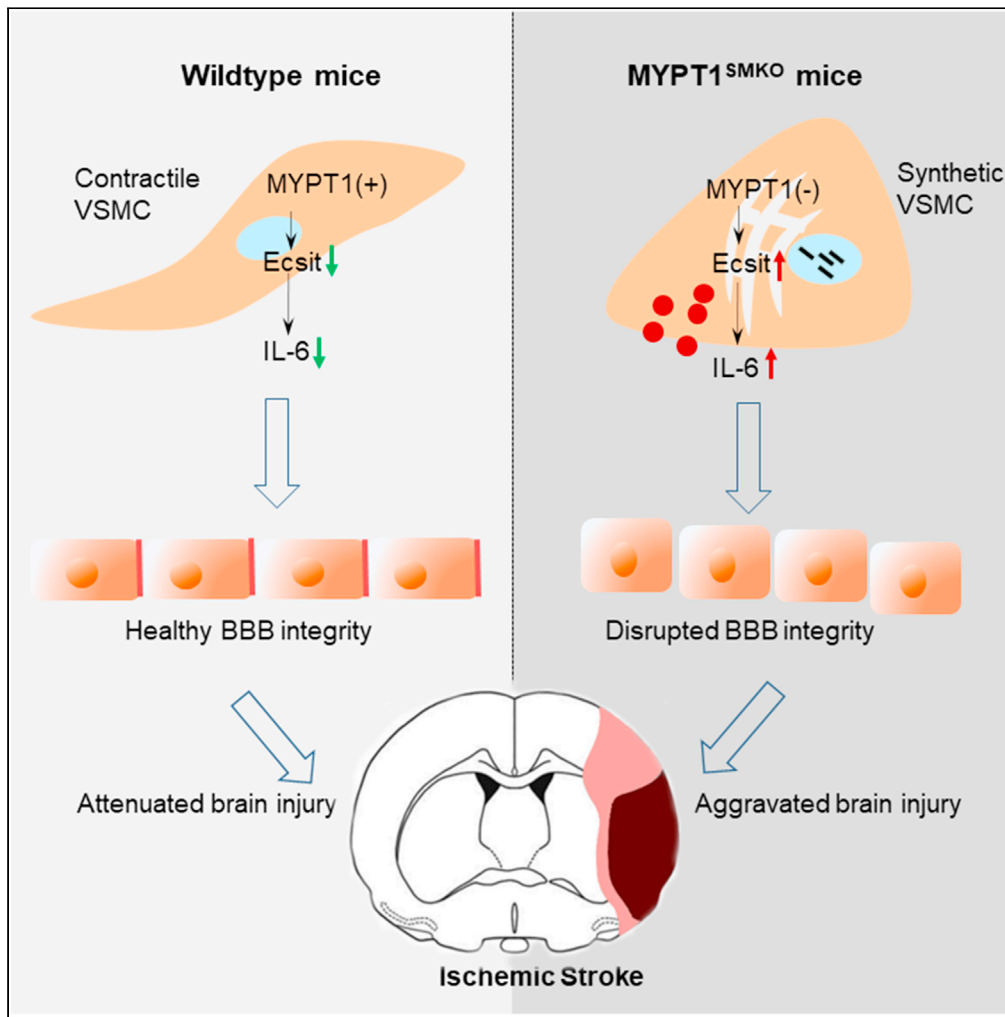


Article

Synthetic VSMCs induce BBB disruption mediated by MYPT1 in ischemic stroke



Hailan Meng,
Lizhen Fan, Cun-
Jin Zhang, ...,
Zhijun Pu, Min-
Sheng Zhu, Yun Xu

xuyun20042001@aliyun.com

Highlights

MYPT1 deficiency induces activation of synthetic VSMCs and aggravates BBB disruption

Synthetic VSMCs release more IL-6 to destroy BBB in a contact-independent way

MYPT1-ECSIT-IL-6 signaling pathway regulates synthetic VSMC-mediated BBB disruption



Article

Synthetic VSMCs induce BBB disruption mediated by MYPT1 in ischemic stroke

Hailan Meng,^{1,2,3,4,5} Lizhen Fan,^{1,2,3,4,5} Cun-Jin Zhang,^{1,2,3,4,5} Liwen Zhu,^{1,2,3,4,5} Pinyi Liu,^{1,2,3,4,5} Jian Chen,^{1,2,3,4,5} Xinyu Bao,^{1,2,3,4,5} Zhijun Pu,^{1,2,3,4,5} Min-Sheng Zhu,^{6,7} and Yun Xu^{1,2,3,4,5,8,*}

SUMMARY

Vascular smooth muscle cells (VSMCs) have been widely recognized as key players in regulating blood-brain barrier (BBB) function, and their roles are unclear in ischemic stroke. Myosin phosphatase target subunit 1 (MYPT1) is essential for VSMC contraction and maintaining healthy vasculature. We generated VSMC-specific MYPT1 knockout (MYPT1^{SMKO}) mice and cultured VSMCs infected with Lv-shMYPT1 to explore phenotypic switching of VSMCs and the accompanied impacts on BBB integrity. We found that MYPT1 deficiency induced phenotypic switching of synthetic VSMCs, which aggravated BBB disruption. Proteomic analysis identified evolutionarily conserved signaling intermediates in Toll pathways (ECSIT) as a downstream molecule that promotes activation of synthetic VSMCs and contributed to IL-6 expression. Knocking down ECSIT rescued phenotypic switching of VSMCs and BBB disruption. Additionally, inhibition of IL-6 decreased BBB permeability. These findings reveal that MYPT1 deficiency activated phenotypic switching of synthetic VSMCs and induced BBB disruption through ECSIT-IL-6 signaling after ischemic stroke.

INTRODUCTION

Ischemic stroke is one of the leading causes of death worldwide, and survivors often suffer from long-lasting disabilities (Benjamin et al., 2017). The treatment of ischemic stroke remains a clinical challenge; thus, exploration of novel therapeutic strategies is urgently needed. It is generally accepted that the blood-brain barrier (BBB) plays an important role in the early development of ischemic stroke and is a potential target for the treatment of ischemic stroke (Thrippleton et al., 2019). Cerebral vasculature dysfunction, along with extracellular matrix degradation and subsequent inflammatory responses, contributes to driving BBB disruption after ischemic stroke (Thrippleton et al., 2019; Liebner et al., 2018). However, the mechanisms underlying the changes in BBB integrity and the effects of these changes on ischemic stroke outcomes remain ill-defined.

Although BBB is mainly composed of endothelial cells, astrocytes, and pericytes, it has been evidenced that vascular smooth muscle cells (VSMCs) also contribute to the integrity of BBB (Zhao et al., 2015). As one of the major cell types in the cerebral vasculature, VSMCs help to stabilize the BBB integrity and maintain healthy vasculature (Liebner et al., 2018). Dysfunction of VSMCs may induce impairment of the myogenic response and cerebral autoregulation, which further evokes BBB leakage and causes neuronal death and synaptic dysfunction, resulting in neurological deficits (Shekhar et al., 2017; Merlini et al., 2011; Kanekiyo et al., 2012). In many vascular disorders, VSMCs can switch from a quiescent contractile phenotype to an active synthetic phenotype, and VSMCs with an active synthetic phenotype synthesize and secrete proinflammatory factors and matrix proteins, leading to vascular integrity disruption (Shen et al., 2019). However, the pathological role and molecular mechanisms of VSMCs in the maintenance of BBB integrity after ischemic stroke remain elusive and must be further investigated.

Myosin phosphatase target subunit 1 (MYPT1), the regulatory subunit of myosin light chain phosphatase, plays an essential role in smooth muscle contraction by modulating phosphorylation of the Ca²⁺-dependent myosin regulatory light chain (Qiao et al., 2014). Accumulating data suggest that MYPT1 plays an important role in other noncontractile functions, including cell migration or adhesion, cell proliferation, cell division, neurotransmitter release, embryonic development, and regulation of endothelial and

¹Department of Neurology of Drum Tower Hospital, Medical School and the State Key Laboratory of Pharmaceutical Biotechnology, Nanjing University, Nanjing 210008, China

²Institute of Brain Sciences, Nanjing University, Nanjing 210008, China

³Jiangsu Key Laboratory for Molecular Medicine, Medical School of Nanjing University, Nanjing 210008, China

⁴Jiangsu Province Stroke Center for Diagnosis and Therapy, Nanjing 210008, China

⁵Nanjing Neuropsychiatry Clinic Medical Center, Nanjing 210008, China

⁶Model Animal Research Center, Nanjing University, Nanjing 210061, China

⁷Ministry of Education (MOE) Key Laboratory of Model Animal for Disease Study, Nanjing University, Nanjing 210061, China

⁸Lead contact

*Correspondence: xuyun20042001@aliyun.com
<https://doi.org/10.1016/j.isci.2021.103047>



epithelial barrier function (Kiss et al., 2019; Eto, 2009). However, little is known about the effects of MYPT1 in regulating the phenotypic switching of VSMCs and their impacts on BBB integrity and the neurological outcomes after ischemic stroke.

In the current study, we explored the role of MYPT1 deficiency in the phenotypic switching of VSMCs and it subsequently influences in modulating BBB integrity after ischemic stroke. Here, we provided evidence that synthetic VSMCs aggravate BBB disruption in a contact-independent way in acute ischemic stroke. MYPT1 deficiency promotes the phenotypic switching of synthetic VSMCs accompanied with increased IL-6 expression and aggravates BBB disruption after ischemic stroke. In addition, we found that evolutionarily conserved signaling intermediates in Toll pathways (ECSIT) is a downstream molecule of MYPT1 that is involved in phenotypic switching of VSMCs and contributes to IL-6 expression.

RESULTS

VSMC-specific MYPT1 deficiency increases the brain infarct size and neurological deficits after ischemic stroke

To determine the role of VSMC-specific MYPT1 in ischemic brain injury, age- and sex-matched MYPT1^{SMKO} and WT mice were subjected to middle cerebral artery occlusion (MCAO) for 60 min followed by reperfusion at 1 d, 3 d, and 7 d. Data from laser speckle imaging technology show that there is no significant difference in cerebral blood flow between MYPT1^{SMKO} and WT mice both upon ischemia as well as during reperfusion (Figure S1). Triphenyl tetrazolium chloride (TTC) staining was performed to evaluate the cerebral infarct volume. MYPT1^{SMKO} mice showed significantly larger infarcts than WT mice 1, 3, and 7 d after MCAO (Figures 1A and 1B). Consistently, MYPT1^{SMKO} mice exhibited worse performance than WT mice in the modified neurological severity score (mNSS) test, rotarod test, foot fault test, and forelimb grip strength test 1, 3, and 7 d after MCAO, indicating severe deficits in motor function, sensorimotor coordination, and muscle strength (Figures 1C–1F). It is worth noting that the neurological deficits of MYPT1^{SMKO} mice were the worst 1 d after MCAO and that BBB disruption peaked at 1 d after MCAO, which is consistent with previous reports (Chang et al., 2017); therefore, 1 d after MCAO was chosen as the main time point in the subsequent experiments.

VSMC-specific MYPT1 deficiency exacerbates ischemia-induced BBB disruption

To test whether VSMC-specific MYPT1 deficiency aggravates the disruption of BBB permeability after ischemic stroke, we quantified Evans blue (EB) extravasation and fluorescein isothiocyanate (FITC)-dextran labeling *in vivo*. The results showed increased EB and FITC-dextran leakage in the ischemic hemisphere in MYPT1^{SMKO} mice 1 d after MCAO (Figures 2A–2D). Since tight junction (TJ) proteins in endothelial cells are important for maintaining BBB function (Kunze and Marti, 2019), we further evaluated the protein expression of ZO-1, occludin, and claudin-5 by immunofluorescence and western blotting. As shown in Figures 2E–2G, compared with wild type (WT) mice, the alignment of TJs in endothelial cells was severely impaired in the ischemic hemisphere in MYPT1^{SMKO} mice 1 d after MCAO. Consistently, western blotting analysis confirmed that the protein expression levels of ZO-1, occludin, and claudin-5 were significantly reduced in the ischemic hemisphere of MYPT1^{SMKO} mice 1 d after MCAO (Figures 2I and 2J). Furthermore, in electron microscopic scanning, endothelial swelling and TJ loss were observed in the cortical arterioles of MYPT1^{SMKO} and WT mice 1 d after MCAO but not in the two sham groups; in MYPT1^{SMKO} mice, TJ loss in cortical arterioles was more severe than in WT mice, and TJs were irregularly distributed (Figure 2H). Notably, the VSMCs of MYPT1^{SMKO} mice contained more cell organelles than those of WT mice 1 d after MCAO, which indicates that VSMCs with MYPT1 deficiency may undergo phenotypic switching during acute ischemic stroke (Figure 2H).

MYPT1 deficiency induces the switching of cerebral VSMCs to the synthetic phenotype after ischemic stroke

To validate the roles of MYPT1 in modulating the phenotypic switching of VSMCs after ischemia, we silenced MYPT1 expression in cultured human brain vascular smooth muscle cells (HBVSMCs) transfected with lentivirus before subjected to OGD/R *in vitro*. Specific markers of the contractile phenotype of VSMCs, including α -SMA, SM22 α , and calponin, were selected for further validation as reported previously (Zeng et al., 2019; Yang et al., 2017). The transduction efficiency of Lv-shMYPT1 was determined by immunofluorescence, western blotting, and Q-PCR (Figures S2A–S2D). Both Lv-shMYPT1-1 and Lv-shMYPT1-2 were effective in silencing MYPT1 expression in HBVSMCs. Lv-shMYPT1-1, which exhibited higher efficiency, was selected for further experiments. After 4 hr of oxygen-glucose deprivation (OGD) followed by 24 hr of reoxygenation, both the mRNA and protein levels of contractile phenotype markers (α -SMA, SM22 α , and calponin) and MYPT1 expression were significantly

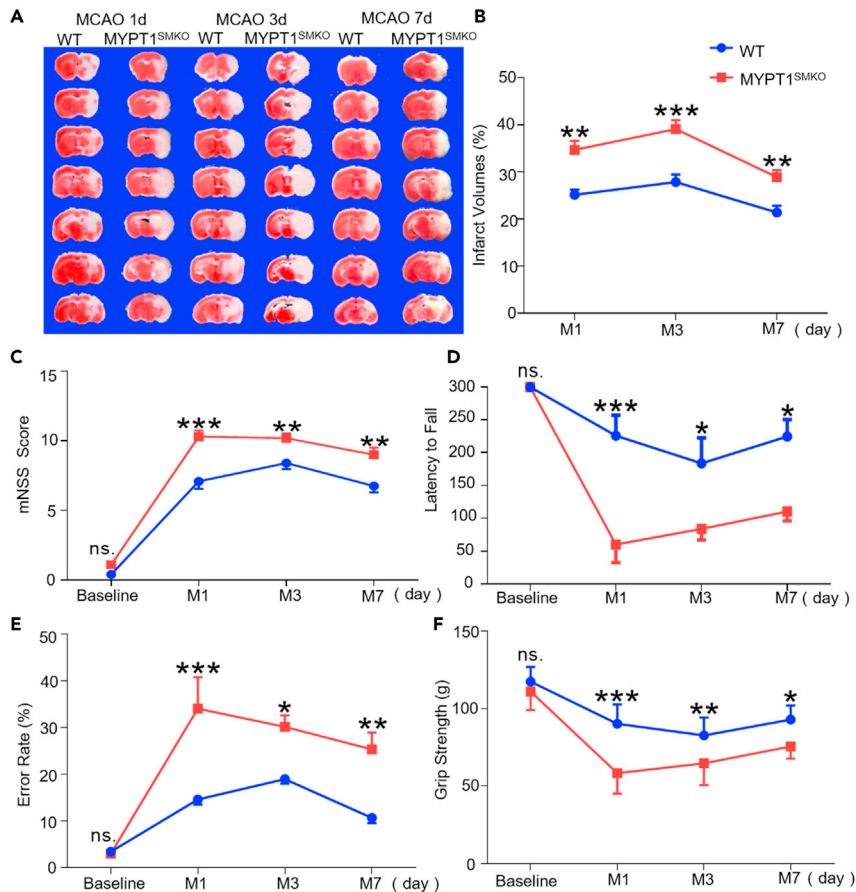


Figure 1. VSMC-specific MYPT1 deficiency increases the brain infarct size and neurological deficits after ischemic stroke

(A and B) Analysis of the infarct volume in WT and MYPT1^{SMKO} mice 1 d, 3 d, and 7 d after MCAO by TTC staining and quantification. $n = 4-7$.

(C-F) Performance of WT and MYPT1^{SMKO} mice in the mNSS test, the rotarod test, foot fault test, and the forelimb grip strength test 1 d, 3 d, and 7 d after MCAO. $n = 10$. Data are represented as mean \pm SEM. * $p < 0.05$, ** $p < 0.01$ and *** $p < 0.001$. Two-way ANOVA followed by Tukey's test for multiple comparisons was used to analyze the difference between two groups at more than one time point.

upregulated in HBVSMCs (Figures 3A-3C). However, MYPT1 deficiency decreased the mRNA and protein levels of these contractile phenotype markers (Figures 3A-3C). Immunofluorescence staining consistently showed that the expression of α -SMA and SM22 α in HBVSMCs was decreased in the MYPT1-deficient HBVSMCs after OGD (Figure 3D). In addition, the changes in MYPT1, α -SMA, SM22 α , and calponin protein expression were confirmed in cortical arterioles in MYPT1^{SMKO} mice after MCAO (Figures 3F and 3G). Furthermore, to evaluate the switching of VSMCs to the synthetic phenotype, we measured the levels of the main cytokines secreted by HBVSMCs, including IL-8, IL-1 β , IL-6, IL-10, TNF- α , and IL-12p70, as reported previously (Shi et al., 2020; Luo et al., 2020). In the OGD/R models, although the levels of both IL-8 and IL-6 in the supernatant of HBVSMCs were in high levels, as determined by the CBA Inflammation Kit, IL-6 was the only cytokine secreted by MYPT1-deficient HBVSMCs that was upregulated (Figure 3E). Taken together, these data demonstrate that MYPT1 contributes to the phenotypic switching of VSMCs after ischemia and that depletion of MYPT1 in VSMCs suppresses phenotypic switching to the contractile phenotype and promotes IL-6 secretion.

MYPT1 deficiency enhances BBB disruption induced by synthetic VSMCs after ischemic stroke

To explore the effects of MYPT1-deficient synthetic VSMCs on BBB integrity, the supernatant of human brain microvascular endothelial cells (HBVSMCs) transfected with or without Lv-shMYPT1 was collected

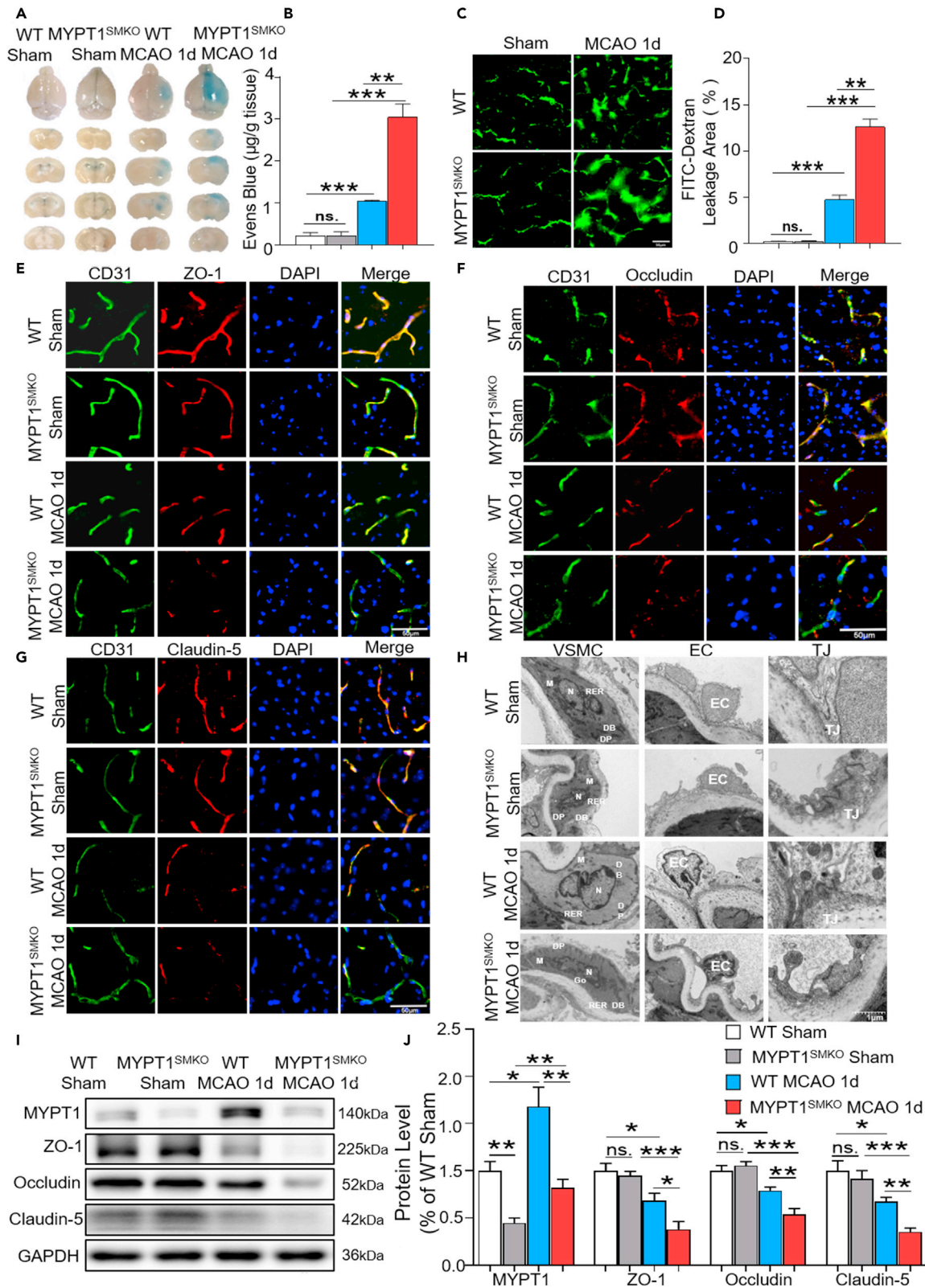


Figure 2. VSMC-specific MYPT1 deficiency promotes ischemia-induced BBB disruption

(A and B) EB staining and quantification in WT and MYPT1^{SMKO} mice from the sham groups and 1 d MCAO groups. n = 3.
(C and D) Representative images and quantification of FITC-dextran (70 kDa) leakage in WT and MYPT1^{SMKO} mice from the sham groups and 1 d MCAO groups. Scale bar: 50 μ m. n = 5.
(E–G) Representative double immunofluorescence staining for ZO-1, occludin, and claudin-5 with CD31 in WT and MYPT1^{SMKO} mice from the sham groups and 1 d MCAO groups. Scale bar: 50 μ m.
(H) Representative scanning electron microscopy images of VSMCs, endothelial cells, and TJs in the cortical arterioles of WT and MYPT1^{SMKO} mice from the sham groups and 1 d MCAO groups. Scale bar: 1 μ m. VSMCs: vascular smooth muscle cells. ECs: endothelial cells. TJ: tight junction. M: mitochondria. N: nucleus. RER: rough ER. DB: dense body. DP: dense patch. Go: Golgi apparatus.
(I and J) Western blotting and quantification of MYPT1, ZO-1, occludin, and claudin-5 expression in the cortical arterioles of WT and MYPT1^{SMKO} mice from the sham groups and 1 d MCAO groups. n = 5. Data are represented as mean \pm SEM. *p < 0.05, **p < 0.01 and ***p < 0.001 by one-way ANOVA and Bonferroni's post hoc test.

and used to stimulate monolayer HBMECs after OGD/R. In addition to TJs, VE-cadherin plays a central role in controlling endothelial barrier function, which is transiently disrupted by proinflammatory cytokines after stroke (Colás-Algora et al., 2020). Immunofluorescence staining for VE-cadherin, ZO-1, and claudin-5 showed that BBB integrity was disrupted when HBMECs were treated with the supernatant of HBVSMCs after OGD/R, which indicated that synthetic VSMCs were deleterious to BBB integrity. In addition, BBB integrity was further disrupted when HBMECs were treated with the supernatant of HBVSMCs transfected with Lv-shMYPT1 (Figure 4A). Consistently, the protein levels of ZO-1, occludin, and claudin-5 in HBMECs treated with the supernatant of HBVSMCs with transfected Lv-shMYPT1 were significantly downregulated (Figures 4B and 4C). In addition, FITC-dextran permeability was increased, and the transendothelial electrical resistance (TEER) value was decreased when HBMECs were stimulated with the supernatant of HBVSMCs with transfected Lv-shMYPT1 (Figures 4D and 4E). Therefore, we concluded that MYPT1 knockdown in VSMCs exacerbates BBB disruption after ischemic stroke.

ECSIT is involved in MYPT1 signaling in cerebral VSMCs after ischemic stroke

To comprehensively understand the mechanism by which MYPT1 modulates the phenotypic switching of VSMCs after ischemic stroke, the proteins of cortical small vessel from MYPT1^{SMKO} and WT mice subjected to MCAO or the sham group were collected for proteomic screening. Notably, cortical arterioles were collected for proteomic analysis instead of cerebral VSMCs because it was difficult to isolate pure cerebral VSMCs and because data from *in vivo* tissue samples are more convincing than data from cell lines *in vitro*. Protein expression was analyzed with the Human Protein Atlas (<http://www.proteinatlas.org/>), and further *in vivo* and *in vitro* validation experiments were performed.

In total, 5770 proteins were identified by proteomic screening. Proteins that exhibited a 1.2 times change in expression and had a t test p value < 0.05 were considered as differential expression proteins (DEPs). DEPs involved in VSMC function were selected and were shown in the corresponding heatmap. ECSIT was one of the most obviously increased proteins in the MYPT1^{SMKO} WT mice 1 d after MCAO and was highly expressed in VSMCs (Figure 5A). Q-PCR and western blotting further verified that the mRNA and protein levels of ECSIT were increased in the MYPT1^{SMKO} and WT mice 1 d after MCAO (Figures 5B–5D). Changes in ECSIT expression levels were also validated in the *in vitro* models. The levels of ECSIT were significantly increased in MYPT1-deficient HBVSMCs after OGD, as detected by both Q-PCR and western blotting (Figures 5E–5G). Taken together, these data reveal that ECSIT is involved in MYPT1 signaling in cerebral VSMCs following ischemic stroke.

ECSIT silencing inhibits switching in MYPT1-deficient VSMCs to the synthetic phenotype and ameliorates BBB disruption after ischemic stroke

To further explore the role of ECSIT in MYPT1-mediated phenotypic switching of VSMCs after OGD exposure, we subjected Lv-shMYPT1-transfected HBVSMCs to siRNA-mediated ECSIT knockdown. The siRNA knockdown efficiency was shown in Figures S2E–S2G. Both the mRNA and protein expression levels of ECSIT were significantly decreased in MYPT1-deficient HBVSMCs, as determined by Q-PCR and western blotting (Figures 6A–6C). Although the mRNA expression of markers of the contractile phenotype (α -SMA, SM22 α , and calponin) was decreased in MYPT1-deficient HBVSMCs subjected to OGD, ECSIT silencing rescued the expression of these genes (Figure 6A). Similar changes in protein levels were found by western blotting (Figures 6B and 6E–6G). In addition, the IL-6 levels in the supernatant of MYPT1-deficient HBVSMCs were dramatically decreased after ECSIT silencing (Figure 6H). These data demonstrate

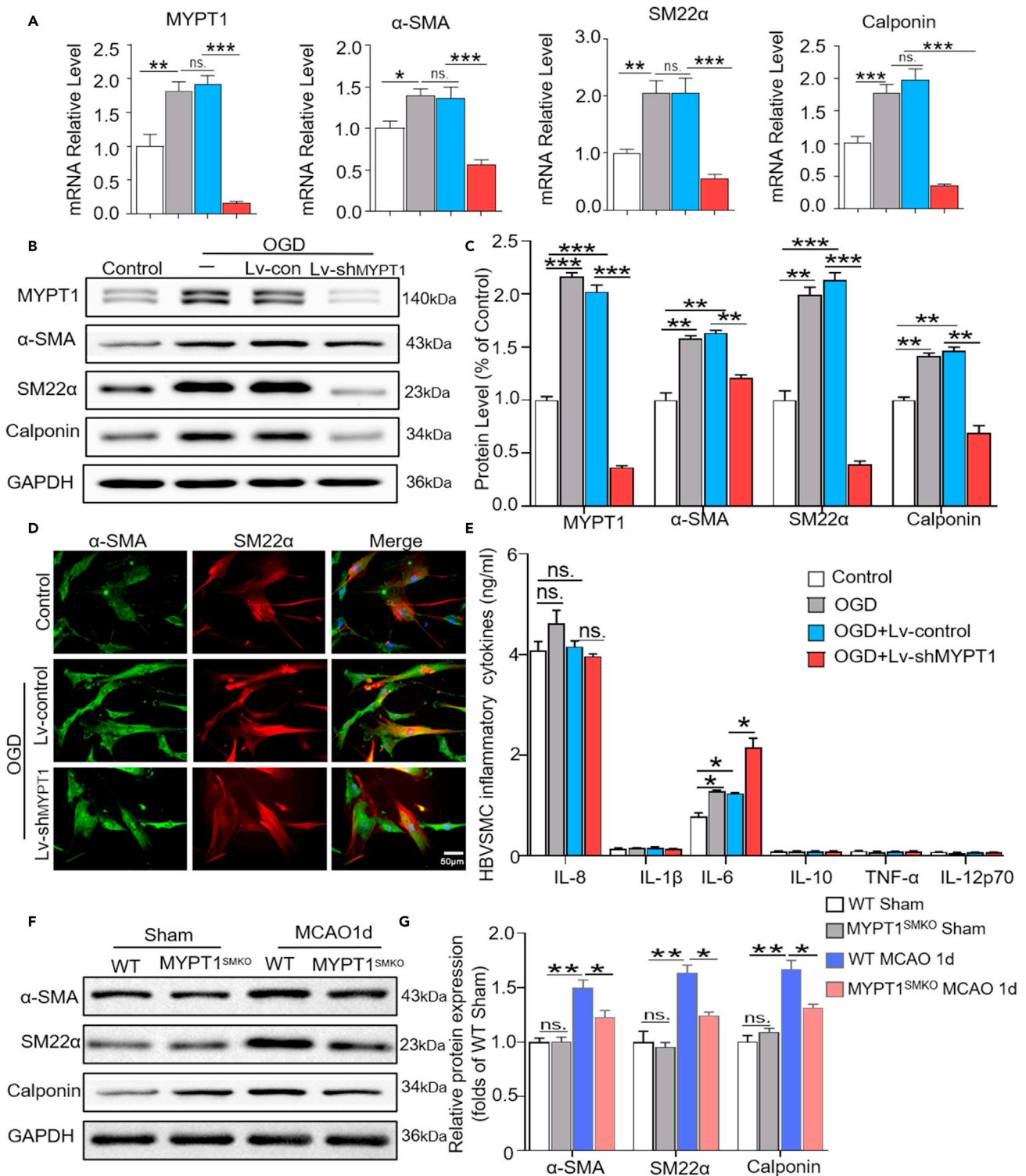


Figure 3. MYPT1 deficiency facilitates the switching of cerebral VSMCs to the synthetic phenotype after ischemic stroke

(A) The mRNA levels of MYPT1, α-SMA, SM22α, and calponin in HBVSMCs from the control, OGD, OGD+Lv-control, and OGD+Lv-shMYPT1 groups. n = 9. (B and C) Western blot analysis and quantification of MYPT1, α-SMA, SM22α, and calponin in HBVSMCs from the control, OGD, OGD+Lv-control, and OGD+Lv-shMYPT1 groups. n = 3. (D) Representative immunofluorescence staining for α-SMA and SM22α in HBVSMCs from the control, OGD, OGD+Lv-control, and OGD+Lv-shMYPT1 groups. Scale bar: 50 μm.

Figure 3. Continued

(E) Inflammatory cytokine levels in HBVSMCs from the control, OGD, OGD+Lv-control, and OGD+Lv-shMYPT1 groups. n = 3.

(F–G) Western blot analysis and quantification of α -SMA, SM22 α , and calponin expression in the cortical arterioles of WT and MYPT1^{SMKO} mice from the sham groups and 1 d MCAO groups. n = 3. Data are represented as mean \pm SEM. *p < 0.05, **p < 0.01, and ***p < 0.001 by one-way ANOVA and Bonferroni's post hoc test. HBVSMCs: human brain vascular smooth muscle cells. OGD: oxygen-glucose deprivation. Lv-control: control lentivirus. Lv-shMYPT1: MYPT1-inhibiting lentivirus.

the critical role of ECSIT in phenotypic switching of VSMCs mediated by the MYPT1 pathway after ischemic stroke.

To determine whether ECSIT-mediated phenotypic switching of VSMCs influences BBB disruption after ischemic injury, HBMECs were subjected to OGD/R and then treated with the supernatants of HBVSMCs from different groups. As described above, the supernatant of MYPT1-deficient HBVSMCs aggravated BBB disruption. However, the protein levels of ZO-1, occludin, and claudin-5 in HBMECs treated with the supernatant of MYPT1-deficient HBVSMCs were slightly increased after ECSIT silencing (Figures 6I–6L). Additionally, FITC-dextran permeability was decreased, and TEER values were increased when HBMECs were treated with the supernatant of MYPT1-deficient HBVSMCs after ECSIT silencing (Figures 6M and 6N). These data illustrate that ECSIT might play an important role in the phenotypic switching of MYPT1-deficient HBVSMCs and that ECSIT silencing could partly rescue the aggravation of BBB disruption by MYPT1-deficient HBVSMCs subjected to OGD *in vitro*.

IL-6 plays an important role in BBB disruption mediated by the MYPT1-ECSIT pathway

As mentioned above, IL-6 was the most significantly altered cytokine in the supernatant of MYPT1-deficient HBVSMCs. Thus, we hypothesized that IL-6 is the key cytokine for modulating BBB function through MYPT1-ECSIT-mediated phenotypic switching of VSMCs. Firstly, HBMECs were treated with exogenous IL-6 and with or without tocilizumab, a specific IL-6R-neutralizing antibody, to confirm the direct modulatory effect of IL-6 on BBB integrity. As expected, the protein levels of ZO-1, occludin, and claudin-5 were decreased in HBMECs treated with IL-6 compared to control HBMECs but were increased when IL-6R was blocked with tocilizumab (Figures 7A and 7B). As indicated by FITC-dextran labeling and TEER analysis, the permeability of HBMECs was increased upon treatment with IL-6 and decreased when IL-6R was blocked with tocilizumab (Figures 7C and 7D), which indicates that IL-6 can directly disrupt BBB integrity. Furthermore, we found that when HBVSMCs were treated with tocilizumab, the protein levels of ZO-1, occludin, and claudin-5 in HBMECs treated with the supernatant of MYPT1-deficient HBVSMCs subjected to OGD were significantly increased (Figures 7E and 7F). Accordingly, the permeability of HBMECs treated with the supernatant of MYPT1-deficient HBVSMCs was decreased after treatment with tocilizumab (Figures 7G and 7H).

To determine whether the results obtained from inhibitory experiments of IL-6 in HBVSMCs *in vitro* can be translated into therapy *in vivo*, tocilizumab and PBS were injected intraperitoneally into MYPT1^{SMKO} mice 1 d after MCAO. There was a decrease in EB and FITC-dextran leakage in MYPT1^{SMKO} mice injected with tocilizumab (Figures 7I–7L). Consistently, western blotting showed that the protein levels of ZO-1, occludin, and claudin-5 were slightly increased in the ischemic cortical arterioles of MYPT1^{SMKO} mice injected with tocilizumab (Figures 7M and 7N). These results demonstrated that IL-6 might play an important role in synthetic VSMC-mediated BBB disruption after ischemic stroke.

DISCUSSION

In this study, we explored the potential role of endogenous MYPT1 in VSMCs and the involvement in modulating BBB disruption after ischemic brain injury. We demonstrated that VSMC-specific MYPT1 deficiency aggravated BBB breakdown in mice after ischemic stroke. We further revealed that MYPT1 deletion promoted the phenotypic switching of synthetic VSMCs and subsequently exerted a detrimental effect on BBB integrity in contact-independent way. Mechanistically, endogenous MYPT1-ECSIT signaling regulated phenotypic switching of synthetic VSMCs and the production of IL-6 in VSMCs after ischemic stroke.

MYPT1, which interacts with PP1c to form the MP holoenzyme and modulates Ca²⁺-dependent phosphorylation of myosin light chain by myosin light-chain kinase, is essential for modulating contraction in VSMCs and contributes to blood flow maintenance (Al-Shboul et al., 2014). MYPT1 can also binds to certain substrates to bring the substrate and the catalytic subunit together, which effectively dephosphorylates the

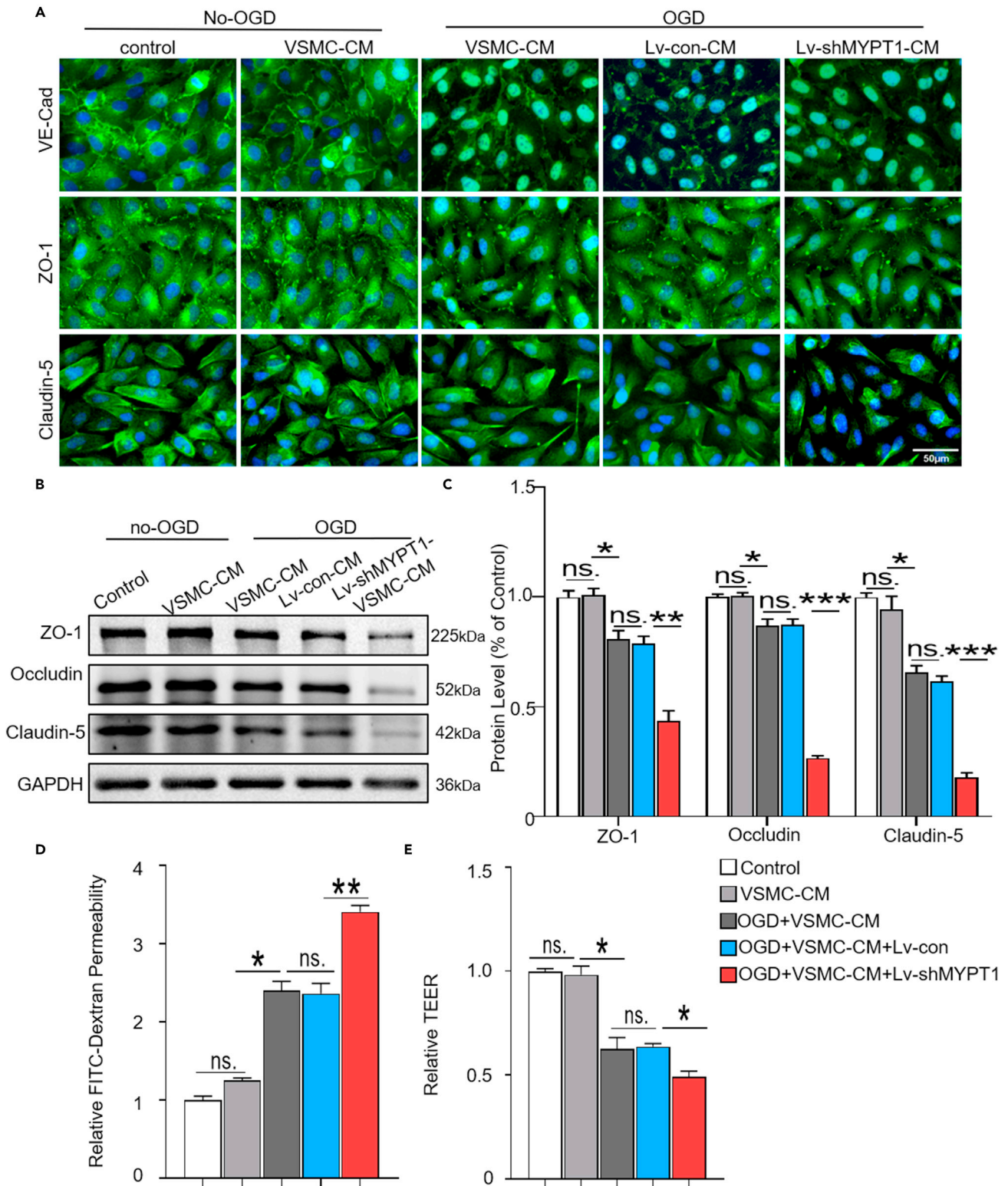


Figure 4. MYPT1 deficiency exacerbates BBB disruption induced by synthetic VSMCs after ischemic stroke

(A) Representative immunofluorescence staining for VE-Cad, ZO-1, and occludin in HBMECs from the control, VSMC-CM, OGD+VSMC-CM, OGD+VSMC-CM+Lv-control, and OGD+VSMC-CM+Lv-shMYPT1 groups. Scale bar: 50 μ m.

Figure 4. Continued

(B and C) Western blot analysis and quantification of MYPT1, ZO-1, occludin, and claudin-5 in HBMECs from the control, VSMC-CM, OGD+VSMC-CM, OGD+VSMC-CM+Lv-control, and OGD+VSMC-CM+Lv-shMYPT1 groups. n = 3.

(D) FITC-dextran (70 kDa) permeability of HBMECs from the control, VSMC-CM, OGD+VSMC-CM, OGD+VSMC-CM+Lv-control, and OGD+VSMC-CM+Lv-shMYPT1 groups. n = 4.

(E) Measurement of TEER in HBMECs from the control, VSMC-CM, OGD+VSMC-CM, OGD+VSMC-CM+Lv-control, and OGD+VSMC-CM+Lv-shMYPT1 groups. n = 6. Data are represented as mean \pm SEM. *p < 0.05, **p < 0.01, and ***p < 0.001 by one-way ANOVA and Bonferroni's post hoc test. HBMECs: human brain microvascular endothelial cells. VSMC-CM: treated with supernatants from VSMCs. TEER: transendothelial electrical resistance.

regulatory light chain of myosin II phosphorylated by ROCK and controls actomyosin contractility in VSMCs. Moreover, MYPT1 has also been shown to dephosphorylate other substrates including adducin, moesin, tau, and MAP2 (Amano et al., 2003; Kimura et al., 1998; Kiss et al., 2019), suggesting that MYPT1 could have broader functions than myosin regulation. As reported, MYPT1 also plays important roles in the development of pathological processes in many diseases, such as the pathology of Huntington disease, depression, intestinal inflammation, pulmonary hypertension, asthma, and insulin resistance (Narayanan et al., 2016; García-Rojo et al., 2017; Al-Shboul et al., 2014; Oka et al., 2007; Yin and Xu, 2018; Taverner et al., 2015). Although many studies have focused on the function of MYPT1 in the regulation of cerebral blood flow, little is known about its potential role in ischemic stroke. In this study, we demonstrated that VSMC-specific MYPT1-deficient mice exhibit larger brain infarctions and more severe neurologic deficits than WT mice after MCAO (Figure 1), which indicate the potential protective roles of MYPT1 in VSMCs after ischemic injury.

Cerebral VSMCs play important roles in brain perfusion maintenance and regulation, which are integral aspects of cerebrovascular autoregulation and homeostasis of the central nervous system (Poittevin et al., 2014). Although VSMCs are not located on the capillaries and do not participate in the component of BBB formation, they contribute to stabilize the BBB integrity and help maintain healthy vasculature (Liebner et al., 2018). Growing evidence have revealed that VSMC-mediated pathogenic processes contribute to BBB destruction in some neurological diseases, such as Alzheimer disease, vascular dementia, cerebral small vessel disease, and arteriovenous malformation (Hainsworth and Markus, 2008; Shekhar et al., 2017). To date, a few studies have elucidated the effect of endothelial cells on VSMCs during different stages of ischemic stroke, which is mediated by catecholamine, acetylcholine, and endothelin expressed by endothelial cells (Poittevin et al., 2014). However, few studies have focused on the influence of VSMCs on endothelial cells and BBB integrity. In this study, we revealed that VSMC-specific MYPT1 deletion changed the morphology and cell organelles in VSMCs and also exacerbated the disruption of BBB permeability and TJ loss in endothelial cells 1 d after MCAO (Figure 2), which indicates that VSMCs are involved in BBB integrity after ischemic stroke.

Considering the physical distance between VSMCs located in cortical arterioles and BBB mainly sited in small capillary (Attwell et al., 2016; Hill et al., 2015), elucidation of the underlying mechanism of VSMCs in regulating BBB integrity is necessary. Under physiological conditions, VSMCs are important components of the vasculature, which are in a state of high differentiation, exhibiting high contractility and low proliferation (Lacolley et al., 2017). Cumulative data have demonstrated that, under pathological conditions, VSMCs tend to switch from a contractile phenotype to other phenotypes, such as synthetic, osteoblastic, and macrophage-like phenotypes (Zhou et al., 2019; Yang et al., 2017). Among VSMCs of different phenotypes, synthetic VSMCs can also be termed inflammatory VSMCs since they can secrete proinflammatory cytokines and adhesion molecules (Wu et al., 2019b; Schnack et al., 2019). Previous studies have revealed that phenotypic switching of synthetic VSMCs is detrimental in many diseases, including atherosclerosis, arterial aneurysm, aortic dissection, and diabetes (Yang et al., 2018; Kono et al., 2018; Shen et al., 2018). Based on these previous findings, we speculated that phenotype switching of MYPT1-deficient VSMCs is also responsible for the BBB destruction after focal cerebral ischemia observed in the present study. Indeed, we revealed that VSMCs switched from a contractile to a synthetic phenotype in both the cortical arterioles of MYPT1 knockout mice and *in vitro* cultured VSMCs with MYPT1 knockdown (Figure 3). In addition, in *in vitro* BBB models, we observed that the endothelial cells display increased transendothelial permeability and decreased TJs proteins levels when triggered by medium collected from MYPT1-knockdown VSMCs (Figure 4), implying that MYPT1-knockdown VSMCs could significantly exacerbate BBB damage in a contact-independent way by secreting specific cytokines. Therefore, we notably demonstrated that MYPT1 deletion promoted synthetic VSMC phenotype switching and subsequently exerted a detrimental effect on BBB integrity after ischemic stroke.

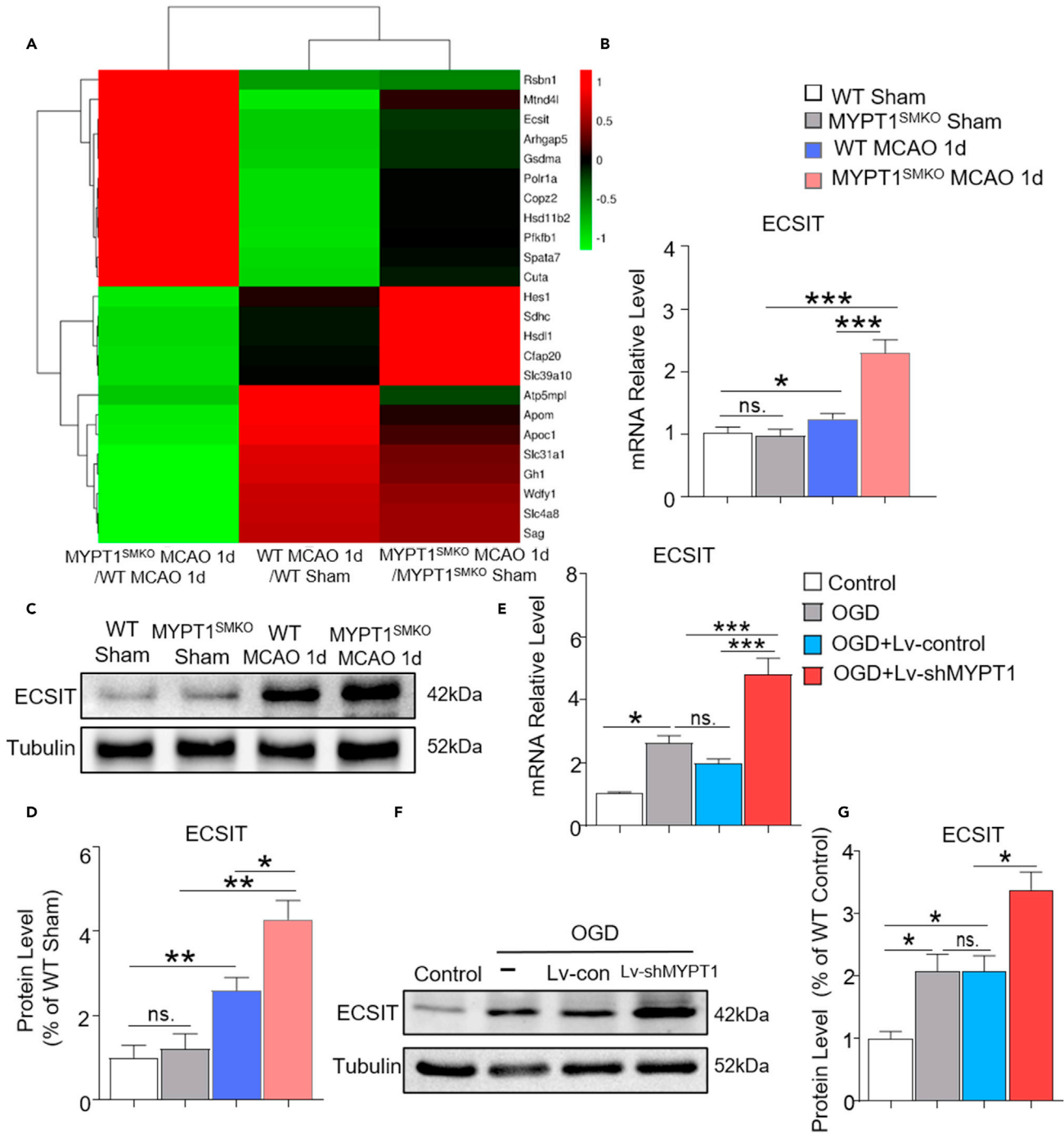


Figure 5. ECSIT is involved in MYPT1 signaling in cerebral VSMCs after ischemic stroke

(A) Heatmap showing the levels of DEPs in the indicated groups.

(B) The mRNA level of ECSIT in the cortical arterioles of WT and MYPT1^{SMKO} mice from the sham groups and 1 d MCAO groups. n = 9.

(C and D) Western blot analysis and quantification of ECSIT in the cortical arterioles of WT and MYPT1^{SMKO} mice from the sham groups and 1 d MCAO groups. n = 4.

(E) The mRNA level of ECSIT in HBVSMCs from the control, OGD, OGD+Lv-control, and OGD+Lv-shMYPT1 groups. n = 9.

(F–G) Western blot analysis and quantification of ECSIT in HBVSMCs from the control, OGD, OGD+Lv-control, and OGD+Lv-shMYPT1 groups. n = 3. Data are represented as mean ± SEM. *p < 0.05, **p < 0.01, and ***p < 0.001 by one-way ANOVA and Bonferroni's post hoc test.

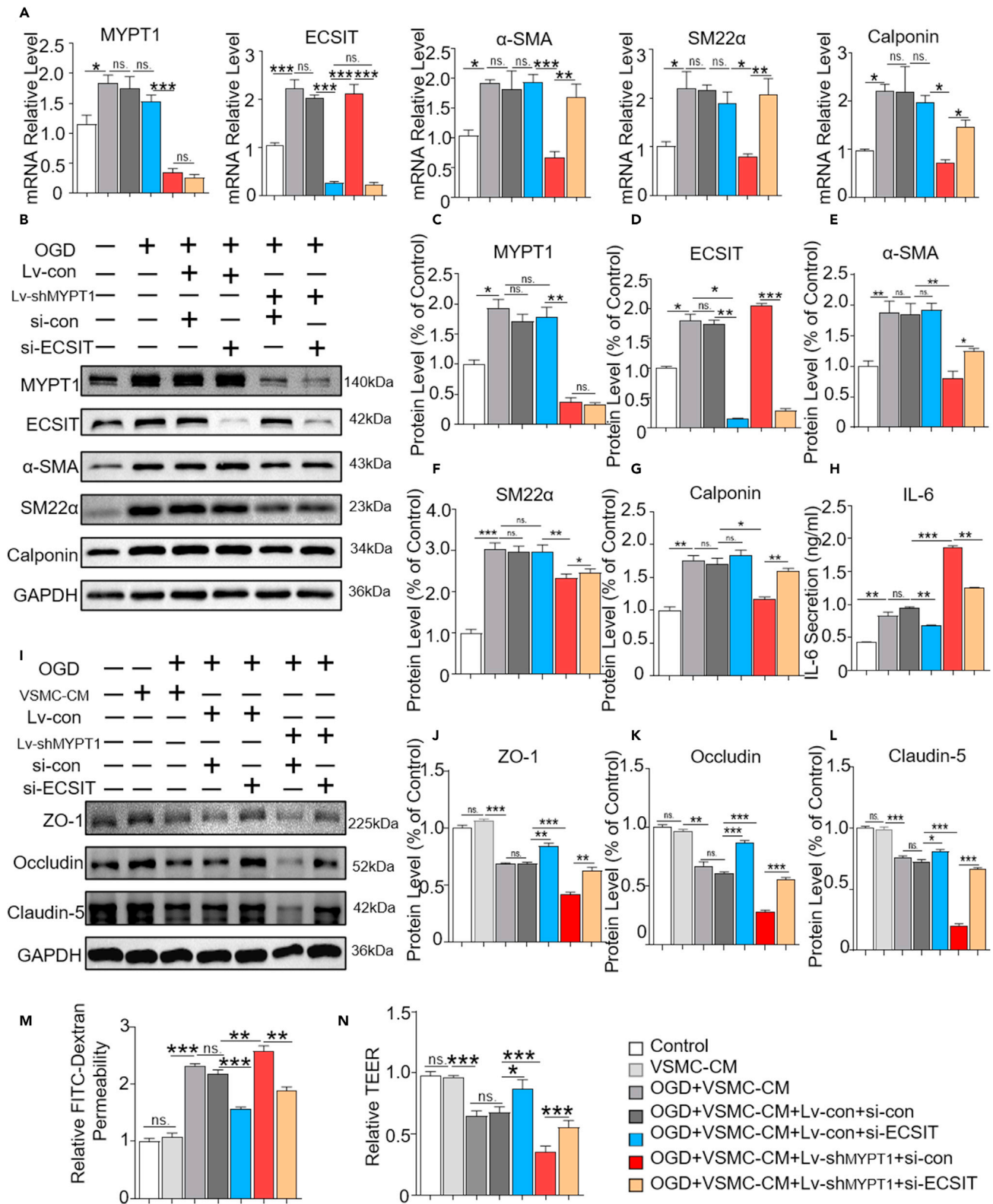


Figure 6. ECSIT silencing inhibits the switching of MYPT1-deficient VSMCs to the synthetic phenotype and ameliorates BBB disruption after ischemic stroke

(A) The mRNA levels of MYPT1, ECSIT, α -SMA, SM22 α , and calponin in HBVSMCs from the control, OGD, OGD+Lv-con+si-control, OGD+Lv-control+si-ECSIT, OGD+Lv-shMYPT1+si-control, and OGD+Lv-shMYPT1+si-ECSIT groups. n = 9.
 (B–G) Western blot analysis and quantification of MYPT1, ECSIT, α -SMA, SM22 α , and calponin expression in HBVSMCs from different groups. n = 3.
 (H) The secretion of IL-6 by HBVSMCs from different groups. n = 6.
 (I–L) Western blot analysis and quantification of ZO-1, occludin, and claudin-5 expression in HBMECs from different groups. n = 3.
 (M) FITC-dextran (70 kDa) permeability of HBMECs from different groups. n = 6.
 (N) Measurement of TEER in HBMECs from different groups. n = 6. Data are represented as mean \pm SEM. *p < 0.05, **p < 0.01, and ***p < 0.00 by one-way ANOVA and Bonferroni's post hoc test. si-con: control siRNA. si-ECSIT: ECSIT-targeting siRNA.

In many vascular disorders, synthetic VSMCs were proven to be detrimental to vascular integrity by synthesizing and secreting proinflammatory factors and matrix proteins, such as IL-6, TNF- α , IL-8, IL-1 β , IL-10, and MCP-1 (Shen et al., 2019). In our study, to evaluate the phenotype switching of synthetic VSMCs and explore the key cytokines, we measured the levels of the main cytokines as reported previously (Shi et al., 2020; Luo et al., 2020). In the OGD/R models, we found that in these cytokines, only IL-8 and IL-6 in the supernatant of HBVSMCs were in high levels. Moreover, IL-6 was the only cytokine secreted by MYPT1-deficient HBVSMCs that was upregulated (Figure 3E), which inspired us to choose IL-6 for further study. It has been widely reported that IL-6 is associated with BBB disruption in a variety of neurological diseases, such as cerebral hemorrhage, mental disorders, and degenerative diseases (Jia et al., 2017; Dong et al., 2016; Orlovskaa-Waast and Köhler-Forsberg, 2019; Watson et al., 2017). In these neurological diseases, IL-6 increases the permeability of the BBB by affecting the adhesion of the endothelium. In HIV-1-associated neurological diseases, STAT1 signaling is activated and induces IL-6 secretion, which leads to decreased expression of claudin-5, ZO-1, and ZO-2 (Chaudhuri et al., 2008). IL-6 can reduce the permeability of TEER and endothelial cells to dyes *in vitro*, while reducing ZO-1 and VE-cadherin immunofluorescence expression, the use of IL-6 neutralizing antibody in *in vitro* experiments can reduce the destruction of the BBB (Gril and Paranjape, 2018). Consistent with the previous studies, in this study, we found that exogenous IL-6 administration obviously exacerbated the disruption of BBB permeability and TJ loss *in vitro* (Figure 7). In contrast, tocilizumab, which inhibits the binding of IL-6 to its receptor, effectively reversed these effects (Figure 7). Our study extends previous findings and demonstrates that synthetic VSMCs promote BBB destruction via the production of IL-6 after ischemic stroke.

ECSIT has been identified as a cytosolic protein that is involved in the inflammatory response and embryonic development. The ECSIT protein is implicated in mitochondrial respiratory chain assembly and interacts with tumor necrosis factor receptor-associated factor 6 (TRAF6), leading to ECSIT ubiquitination and enrichment in the mitochondrial periphery and thus resulting in increased mitochondrial and cellular ROS generation (West et al., 2011). In addition, ECSIT activates the NF- κ B pathway and induces a significant increase in the levels of pro-inflammatory cytokines, including TNF- α , IFN- γ , IL-1 β , and IL-6, in ECSIT-overexpressing immune cells *in vitro* and *in vivo* (Wen et al., 2018). It has been shown that peroxiredoxin-6, p62, and peroxiredoxin-1 can decrease the ubiquitination of ECSIT and inhibit TRAF6 formation and that IL-6 may be associated with activation of the NF- κ B pathway (Min et al., 2017, 2018; Kim et al., 2019), which suggests that ECSIT can promote IL-6 expression by TRAF6 formation and NF- κ B pathway activation. In this study, ECSIT was verified to be the vital molecule that mediated VSMC phenotypic switching and promoted IL-6 secretion (Figures 5 and 6). Our study indicates that MYPT1 deficiency promotes the phenotypic switching of VSMCs in ischemic stroke and exacerbates BBB disruption by the ECSIT-IL-6 pathway.

Classically, the relaxation of VSMCs around arterioles was thought to be important for cerebral autoregulation and control of brain blood flow (Attwell et al., 2010). Recently, it has been clear that pericytes, as spatially isolated contractile cells on capillaries and the main cell component involved in the BBB, also play a key role in regulating cerebral blood flow physiologically, maintaining the integrity of the BBB, regulating immune inflammatory response, participating in angiogenesis, etc. (Peppiatt et al., 2006; Hall et al., 2014). Growing evidence revealed that different subclasses of pericyte along the capillary bed exhibit morphological differences and varied protein expressions play different roles (Attwell et al., 2016): (i) pericytes closer to the arteriole end of the capillary bed express more α -SMA and have more circumferential processes and are likely involved in regulating cerebral blood flow; (ii) pericytes in the middle of the capillary bed that express less α -SMA may be more important for maintaining the BBB function; and (iii) pericytes at the venule end of the capillary bed may regulate immune cell entry to the brain parenchyma. As mentioned above, the subclass of pericytes on capillaries near the arteriole end of the capillary bed express some α -SMA and similar

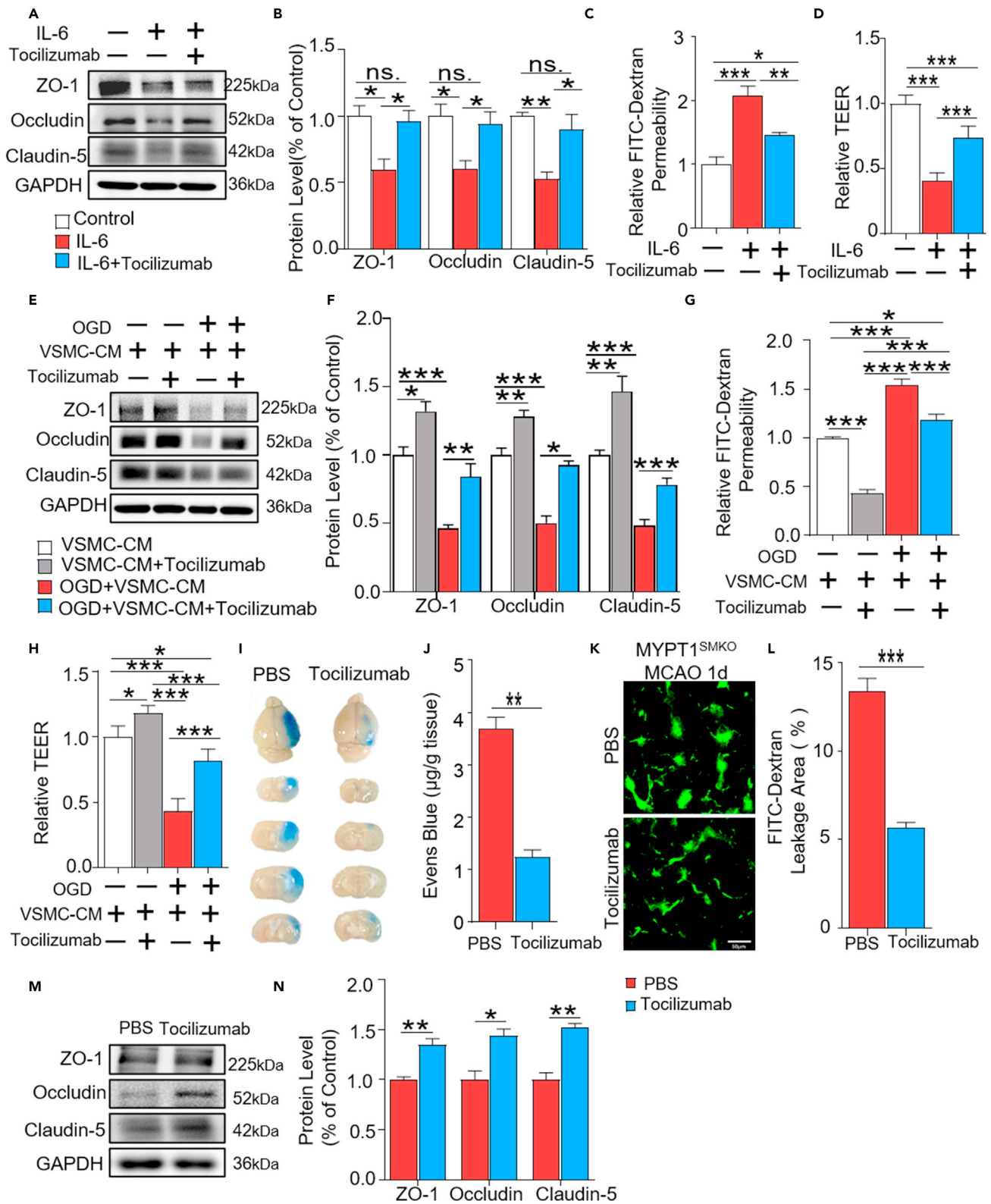


Figure 7. IL-6 plays an important role in BBB disruption mediated by the MYPT1-ECSIT pathway

(A and B) Western blot analysis and quantification of ZO-1, occludin, and claudin-5 expression in HBMECs from the control, IL-6, and IL-6+tocilizumab groups. n = 4.
 (C) FITC-dextran (70 kDa) permeability of HBMECs from the control, IL-6, and IL-6+tocilizumab groups. n = 6.
 (D) Measurement of TEER in HBMECs from the control, IL-6, and IL-6+tocilizumab groups. n = 5.
 (E and F) Western blot analysis and quantification of ZO-1, occludin, and claudin-5 expression in HBMECs from the VSMC-CM+Lv-shMYPT1, VSMC-CM+Lv-shMYPT1+tocilizumab, OGD+VSMC-CM+Lv-shMYPT1, and OGD+VSMC-CM+Lv-shMYPT1+tocilizumab groups. n = 4.
 (G) FITC-dextran (70 kDa) permeability of HBMECs from different groups. n = 6.
 (H) Measurement of TEER in HBMECs from different groups. n = 5.
 (I and J) EB staining and quantification in MYPT1^{SMKO} mice treated with PBS and tocilizumab after MCAO. n = 3.
 (K and L) Representative images and quantification of FITC-dextran (70 kDa) leakage in MYPT1^{SMKO} mice treated with PBS and tocilizumab after MCAO. Scale bar: 50 μ m. n = 5.
 (M and N) Western blot analysis and quantification of ZO-1, occludin, and claudin-5 expression in the cortical arterioles of MYPT1^{SMKO} mice treated with PBS and tocilizumab after MCAO. n = 3. Data are represented as mean \pm SEM. *p < 0.05, **p < 0.01, and ***p < 0.001 by one-way ANOVA and Bonferroni's post hoc test.

morphology to VSMCs (Hill et al., 2015), considering the MYPT1^{SMKO} mice used in this study were generated by crossing with SMA-Cre transgenic mice, we should not ignore effects of this subtype of pericytes in modulating cerebral blood flow and the BBB integrity. Unfortunately, due to lacking the definite protein markers and time limitation, we could not accurately distinguish VSMCs and pericytes and compare their functional differences directly in the present study. Interestingly, we compared changes of cerebral blood flow in MYPT1^{SMKO} mice and WT mice using laser speckle imaging technology, and we found no significant difference between the two kinds of mice in cerebral blood flow both upon ischemia as well as during reperfusion (Figure S1), which might indicate that MYPT1 deficiency had little impacts in cerebral blood flow modulated by VSMCs in arterioles and contractile pericytes in capillary. Strictly, although pericytes involved in maintaining the BBB function in the middle of the capillary bed express less α -SMA, we still need to exclude the potential role of these pericytes in the future. Indeed, to avoid confusing in identifying some pericytes and VSMCs, we should recognize different positions along arterioles and the capillary bed, quantify the differences in protein expression and function of three (or more) sub-classes of pericyte.

In conclusion, our data clearly show that VSMCs and MYPT1 play important roles in BBB integrity after ischemia. We also identified MYPT1-mediated phenotypic switching of VSMCs and activation of ECSIT-IL-6 signaling as major mechanisms responsible for these roles. Elucidating the mechanisms of by which MYPT1 in VSMCs mediates BBB disruption may be important for uncovering the pathogenesis of ischemic stroke. Pharmacological modulation of the MYPT1-ECSIT-IL-6 pathway in VSMCs may be a potential therapeutic strategy for stroke-induced BBB disruption.

Limitations of study

Ischemic brain injury activates a series of time-dependent pathophysiological responses after stroke. Dysfunction of VSMCs not only aggravates BBB disruption occurring shortly after stroke but also induces abnormal angiogenesis at the later stage, which are closely related to the prognosis and mortality of patients with stroke. This study focused on exploring VSMCs with MYPT1 deficiency in modulating BBB integrity at the early phase after ischemia. We demonstrated that MYPT1 deficiency activated synthetic VSMCs and induced BBB disruption through ECSIT-IL-6 signaling. Future studies will need to focus on studying the interaction of MYPT1-deficient VSMCs with delayed angiogenesis after ischemic brain injury. Moreover, we expect additional experiments to distinguish VSMCs and SMA⁺ pericytes in capillary bed and exclude the influence of this subclass of pericytes in modulating blood flow and BBB integrity in the present study.

STAR★ METHODS

Detailed methods are provided in the online version of this paper and include the following:

- KEY RESOURCES TABLE
- RESOURCE AVAILABILITY
 - Lead contact
 - Materials availability
 - Data and code availability
- EXPERIMENTAL MODEL AND SUBJECT DETAILS
 - Animals
- METHOD DETAILS

- Ischemia model in mice
- Behavior tests
- Infarct volume calculation
- Quantitation of BBB permeability
- Electron microscope
- Cortical small vessel preparation
- Western blotting analysis
- RNA isolation and quantitative real-time PCR
- Immunofluorescence staining
- Proteomic analysis
- Cytometric bead array
- Cell cultures
- Ischemic model in vitro
- Lentivirus transfection
- RNA interference
- Measurement of TEER
- FITC-dextran permeability assay
- IL-6 and tocilizumab application

● **QUANTIFICATION AND STATISTICAL ANALYSIS**

SUPPLEMENTAL INFORMATION

Supplemental information can be found online at <https://doi.org/10.1016/j.isci.2021.103047>.

ACKNOWLEDGMENTS

This research was supported by the National Natural Science Foundation of China (Nos, 81701168, 81630028, 82001122, and 81920108017).

AUTHOR CONTRIBUTIONS

H.L.M. performed most experiments, analyzed data, and wrote the manuscript; L.Z.F. contributed to perform experiments and manuscript preparation; C.J.Z. analyzed data and edited the manuscript; L.W.Z., P.Y.L., J.C., and Z.J.P. aided in animal experiments; X.Y.B. helped in cell cultures; M.S.Z. provided MYPT1^{SMKO} mice; Y.X. designed this study and edited the manuscript.

DECLARATION OF INTERESTS

The authors declare no competing interests.

Received: January 29, 2021

Revised: June 14, 2021

Accepted: August 24, 2021

Published: September 24, 2021

REFERENCES

- Al-shboul, O., Nalli, A.D., Kumar, D.P., Zhou, R., Mahavadi, S., Kuemmerle, J.F., Grider, J.R., and Murthy, K.S. (2014). Jun kinase-induced overexpression of leukemia-associated Rho GEF (LARG) mediates sustained hypercontraction of longitudinal smooth muscle in inflammation. *Am. J. Physiol. Cell Physiol.* *306*, C1129–C1141.
- Alamri, F.F., Shoyaib, A.A., Biggers, A., Jayaraman, S., Guindon, J., and Karamyan, V.T. (2018). Applicability of the grip strength and automated von Frey tactile sensitivity tests in the mouse photothrombotic model of stroke. *Behav. Brain Res.* *336*, 250–255.
- Amano, M., Kaneko, T., Maeda, A., Nakayama, M., Ito, M., Yamauchi, T., Goto, H., Fukata, Y., Oshiro, N., Shinohara, A., et al. (2003). Identification of Tau and MAP2 as novel substrates of Rho-kinase and myosin phosphatase. *J. Neurochem.* *87*, 780–790.
- Attwell, D., Buchan, A.M., Charpak, S., Lauritzen, M., Macvicar, B.A., and Newman, E.A. (2010). Glial and neuronal control of brain blood flow. *Nature* *468*, 232–243.
- Attwell, D., Mishra, A., Hall, C.N., O'Farrell, F.M., and Dalkara, T. (2016). What is a pericyte? *J. Cereb. Blood Flow Metab.* *36*, 451–455.
- Benjamin, E.J., Blaha, M.J., Chiuve, S.E., Cushman, M., Das, S.R., Deo, R., de Ferranti, S.D., Floyd, J., Fornage, M., Gillespie, C., et al. (2017). Heart disease and stroke statistics-2017 update: a report from the American Heart Association. *Circulation* *135*, e146–e603.
- Chang, J., Mancuso, M.R., Maier, C., Liang, X., Yuki, K., Yang, L., Kwong, J.W., Wang, J., Rao, V., Vallon, M., et al. (2017). Gpr124 is essential for blood-brain barrier integrity in central nervous system disease. *Nat. Med.* *23*, 450–460.
- Chaudhuri, A., Yang, B., Gendelman, H.E., Persidsky, Y., and Kanmogne, G.D. (2008). STAT1 signaling modulates HIV-1-induced inflammatory responses and leukocyte transmigration across the blood-brain barrier. *Blood* *111*, 2062–2072.

- Chen, J., Sanberg, P.R., Li, Y., Wang, L., Lu, M., Willing, A.E., Sanchez-Ramos, J., and Chopp, M. (2001). Intravenous administration of human umbilical cord blood reduces behavioral deficits after stroke in rats. *Stroke* 32, 2682–2688.
- Colás-Algora, N., García-Weber, D., Cacho-Navas, C., Barroso, S., Caballero, A., Ribas, C., Correas, I., and Millán, J. (2020). Compensatory increase of VE-cadherin expression through ETS1 regulates endothelial barrier function in response to. *TNF α* 77, 2125–2140.
- Dong, Y., Fan, C., Hu, W., Jiang, S., Ma, Z., Yan, X., Deng, C., Di, S., Xin, Z., Wu, G., et al. (2016). Melatonin attenuated early brain injury induced by subarachnoid hemorrhage via regulating NLRP3 inflammasome and apoptosis signaling. *J. Pineal Res.* 60, 253–262.
- Dongsheng, H., Zhuo, Z., Jiamin, L., Hailan, M., Lijuan, H., Fan, C., DAN, Y., HE, Z., and YUN, X. (2016). Proteomic analysis of the Peri-infarct area after human umbilical cord mesenchymal stem cell transplantation in experimental stroke. *Aging Dis.* 7, 623–634.
- Eto, M. (2009). Regulation of cellular protein phosphatase-1 (PP1) by phosphorylation of the CPI-17 family, C-kinase-activated PP1 inhibitors. *J. Biol. Chem.* 284, 35273–35277.
- García-Rojo, G., Fresno, C., Vilches, N., Díaz-Véliz, G., Mora, S., Aguayo, F., Pacheco, A., Parra-Fiedler, N., Parra, C.S., Rojas, P.S., et al. (2017). The ROCK inhibitor fasudil prevents chronic restraint stress-induced depressive-like behaviors and dendritic spine loss in rat hippocampus. *Int. J. Neuropsychopharmacol.* 20, 336–345.
- Gril, B., and Paranjape, A.N. (2018). Reactive astrocytic S1P3 signaling modulates the blood-tumor barrier in brain metastases. *Nat. Commun.* 9, 2705.
- Hainsworth, A.H., and Markus, H.S. (2008). Do in vivo experimental models reflect human cerebral small vessel disease? A systematic review. *J. Cereb. Blood Flow Metab.* 28, 1877–1891.
- Hall, C.N., Reynell, C., Gesslein, B., Hamilton, N.B., Mishra, A., Sutherland, B.A., O’Farrell, F.M., Buchan, A.M., Lauritzen, M., and Attwell, D. (2014). Capillary pericytes regulate cerebral blood flow in health and disease. *Nature* 508, 55–60.
- He, W.Q., Qiao, Y.N., Peng, Y.J., Zha, J.M., Zhang, C.H., Chen, C., Chen, C.P., Wang, P., Yang, X., Li, C.J., et al. (2013). Altered contractile phenotypes of intestinal smooth muscle in mice deficient in myosin phosphatase target subunit 1. *Gastroenterology* 144, 1456–1465, 1465 e1-5.
- Hill, R.A., Tong, L., Yuan, P., Murikinati, S., Gupta, S., and Grutzendler, J. (2015). Regional blood flow in the normal and ischemic brain is controlled by arteriolar smooth muscle cell contractility and not by capillary pericytes. *Neuron* 87, 95–110.
- Jia, L.X., Zhang, W.M., Li, T.T., Liu, Y., Piao, C.M., Ma, Y.C., Lu, Y., Wang, Y., Liu, T.T., Qi, Y.F., and Du, J. (2017). ER stress dependent microparticles derived from smooth muscle cells promote endothelial dysfunction during thoracic aortic aneurysm and dissection. *Clin. Sci. (Lond)* 131, 1287–1299.
- Kanekiyo, T., Liu, C.C., Shinohara, M., Li, J., and Bu, G. (2012). LRP1 in brain vascular smooth muscle cells mediates local clearance of Alzheimer’s amyloid-beta. *J. Neurosci.* 32, 16458–16465.
- Kim, M.J., Min, Y., Kwon, J., Son, J., Im, J.S., Shin, J., and Lee, K.Y. (2019). p62 negatively regulates TLR4 signaling via functional regulation of the TRAF6-ECSIT complex. *Immune Netw.* 19, e16.
- Kimura, K., Fukata, Y., Matsuoka, Y., Bennett, V., Matsuura, Y., Okawa, K., Iwamatsu, A., and Kaibuchi, K. (1998). Regulation of the association of adducin with actin filaments by Rho-associated kinase (Rho-kinase) and myosin phosphatase. *J. Biol. Chem.* 273, 5542–5548.
- Kiss, A., Erdődi, F., and Lontay, B. (2019). Myosin phosphatase: unexpected functions of a long-known enzyme. *Biochim. Biophys. Acta Mol. Cell Res.* 1866, 2–15.
- Kono, T., Tong, X., Taleb, S., Bone, R.N., Iida, H., Lee, C.C., Sohn, P., and Gilon, P. (2018). Impaired store-operated calcium entry and STIM1 loss lead to reduced insulin secretion and increased endoplasmic reticulum stress in the diabetic β -cell. *Diabetes* 67, 2293–2304.
- Kunze, R., and Marti, H.H. (2019). Angioneurins - key regulators of blood-brain barrier integrity during hypoxic and ischemic brain injury. *Prog. Neurobiol.* 178, 101611.
- Lacolley, P., Regnault, V., Segers, P., and Laurent, S. (2017). Vascular smooth muscle cells and arterial stiffening: relevance in development, aging, and disease. *Physiol. Rev.* 97, 1555–1617.
- Liebner, S., Dijkhuizen, R.M., Reiss, Y., Plate, K.H., Agalliu, D., and Constantin, G. (2018). Functional morphology of the blood-brain barrier in health and disease. *Acta Neuropathol.* 135, 311–336.
- Luo, Z., Liao, T., Zhang, Y., Zheng, H., Sun, Q., Han, F., Yang, Z., and Sun, Q. (2020). Triptolide attenuates transplant vasculopathy through multiple pathways. *Front. Immunol.* 11, 612.
- Merlini, M., Meyer, E.P., Ulmann-Schuler, A., and Nitsch, R.M. (2011). Vascular beta-amyloid and early astrocyte alterations impair cerebrovascular function and cerebral metabolism in transgenic arcAbeta mice. *Acta Neuropathol.* 122, 293–311.
- Min, Y., Kim, M.J., Lee, S., Chun, E., and Lee, K.Y. (2018). Inhibition of TRAF6 ubiquitin-ligase activity by PRDX1 leads to inhibition of NFKB activation and autophagy activation. *Autophagy* 14, 1347–1358.
- Min, Y., Wi, S.M., Shin, D., Chun, E., and Lee, K.Y. (2017). Peroxiredoxin-6 negatively regulates bactericidal activity and NF- κ B activity by interrupting TRAF6-ECSIT complex. *Front. Cell Infect. Microbiol.* 7, 94.
- Narayanan, K.L., Chopra, V., Rosas, H.D., Malarick, K., and Hersch, S. (2016). Rho kinase pathway alterations in the brain and leukocytes in Huntington’s disease. *Mol. Neurobiol.* 53, 2132–2140.
- Oka, M., Homma, N., Taraseviciene-Stewart, L., Morris, K.G., Kraskauskas, D., Burns, N., Voelkel, N.F., and Mcmurtry, I.F. (2007). Rho kinase-mediated vasoconstriction is important in severe occlusive pulmonary arterial hypertension in rats. *Circ. Res.* 100, 923–929.
- Orlovska-Waast, S., and Köhler-Forsberg, O. (2019). Cerebrospinal fluid markers of inflammation and infections in schizophrenia and affective disorders: a systematic review and meta-analysis. *Mol. Psychiatry* 24, 869–887.
- Peppiatt, C.M., Howarth, C., Mobbs, P., and Attwell, D. (2006). Bidirectional control of CNS capillary diameter by pericytes. *Nature* 443, 700–704.
- Perez-Riverol, Y., Csordas, A., Bai, J., Bernal-Llinares, M., Hewapathirana, S., Kundu, D.J., Inuganti, A., Griss, J., Mayer, G., Eisenacher, M., et al. (2019). The PRIDE database and related tools and resources in 2019: improving support for quantification data. *Nucleic Acids Res.* 47, D442–D450.
- Poittevin, M., Lozeron, P., Hilal, R., Levy, B.I., merkulova-Rainon, T., and Kubis, N. (2014). Smooth muscle cell phenotypic switching in stroke. *Transl Stroke Res.* 5, 377–384.
- Qiao, Y.N., He, W.Q., Chen, C.P., Zhang, C.H., Zhao, W., Wang, P., Zhang, L., Wu, Y.Z., Yang, X., Peng, Y.J., et al. (2014). Myosin phosphatase target subunit 1 (MYPT1) regulates the contraction and relaxation of vascular smooth muscle and maintains blood pressure. *J. Biol. Chem.* 289, 22512–22523.
- Schnack, L., Sohrabi, Y., Lagache, S.M.M., Kahles, F., Bruemmer, D., Waltenberger, J., and Findeisen, H.M. (2019). Mechanisms of trained innate immunity in oxLDL primed human coronary smooth muscle cells. *Front. Immunol.* 10, 13.
- Shekhar, S., Liu, R., Travis, O.K., Roman, R.J., and Fan, F. (2017). Cerebral autoregulation in hypertension and ischemic stroke: a mini review. *J. Pharm. Sci. Exp. Pharmacol.* 2017, 21–27.
- Shen, M., Hu, M., Fedak, P.W.M., Oudit, G.Y., and Kassiri, Z. (2018). Cell-specific functions of ADAM17 regulate the progression of thoracic aortic aneurysm. *Circ. Res.* 123, 372–388.
- Shen, Y., Chen, X., Chi, C., Wang, H., Xue, J., Su, D., Wang, H., Li, M., Liu, B., and Dong, Q. (2019). Smooth muscle cell-specific knockout of FBW7 exacerbates intracranial atherosclerotic stenosis. *Neurobiol. Dis.* 132, 104584.
- Shi, X., PAN, S., Li, L., Li, Y., Ma, W., Wang, H., Xu, C., Li, L., and Wang, D. (2020). HIX003209 promotes vascular smooth muscle cell migration and proliferation through modulating miR-6089. *Aging (Albany NY)* 12, 8913–8922.
- Shinriki, S., Jono, H., Ota, K., Ueda, M., Kudo, M., Ota, T., Oike, Y., Endo, M., Ibusuki, M., Hiraki, A., et al. (2009). Humanized anti-interleukin-6 receptor antibody suppresses tumor angiogenesis and in vivo growth of human oral squamous cell carcinoma. *Clin. Cancer Res.* 15, 5426–5434.
- Sun, J., Yu, L., Huang, S., Lai, X., Milner, R., and Li, L. (2017). Vascular expression of angiotensin II, α 5 β 1 integrin and tight junction proteins is tightly regulated during vascular remodeling in the post-ischemic brain. *Neuroscience* 362, 248–256.

Taverner, A., Dondi, R., Almansour, K., Laurent, F., Owens, S.E., Eggleston, I.M., Fotaki, N., and Mrsny, R.J. (2015). Enhanced paracellular transport of insulin can be achieved via transient induction of myosin light chain phosphorylation. *J. Control* 210, 189–197.

Thrippleton, M.J., Backes, W.H., Sourbron, S., Ingrisch, M., van Osch, M.J.P., Dichgans, M., Fazekas, F., Ropele, S., Frayne, R., van Oostenbrugge, R.J., et al. (2019). Quantifying blood-brain barrier leakage in small vessel disease: review and consensus recommendations. *Alzheimers Dement.* 15, 840–858.

Watson, N., Ding, B., Zhu, X., and Frisina, R.D. (2017). Chronic inflammation - inflammaging - in the ageing cochlea: a novel target for future presbycusis therapy. *Ageing Res. Rev.* 40, 142–148.

Wen, H., Ma, H., Cai, Q., Lin, S., Lei, X., He, B., and Wu, S. (2018). Recurrent ECSIT mutation encoding V140A triggers hyperinflammation and promotes hemophagocytic syndrome in extranodal NK/T cell lymphoma. *Nat. Med.* 24, 154–164.

West, A.P., Brodsky, I.E., Rahner, C., Woo, D.K., Erdjument-Bromage, H., Tempst, P., Walsh, M.C., Choi, Y., Shadel, G.S., and Ghosh, S. (2011). TLR signalling augments macrophage bactericidal

activity through mitochondrial ROS. *Nature* 472, 476–480.

Wu, N., Zhang, X., Bao, Y., Yu, H., Jia, D., and Ma, C. (2019a). Down-regulation of GASS5 ameliorates myocardial ischaemia/reperfusion injury via the miR-335/ROCK1/AKT/GSK-3 β axis. *J. Cell Mol. Med.* 23, 8420–8431.

Wu, W., Zhang, W., Choi, M., Zhao, J., Gao, P., Xue, M., Singer, H.A., Jourdeuil, D., and LONG, X. (2019b). Vascular smooth muscle-MAPK14 is required for neointimal hyperplasia by suppressing VSMC differentiation and inducing proliferation and inflammation. *Redox Biol.* 22, 101137.

Yang, F., Chen, Q., He, S., Yang, M., Maguire, E.M., An, W., Afzal, T.A., Luong, L.A., Zhang, L., and Xiao, Q. (2018). miR-22 is a novel mediator of vascular smooth muscle cell phenotypic modulation and neointima formation. *Circulation* 137, 1824–1841.

Yang, L., Gao, L., Nickel, T., Yang, J., Zhou, J., Gilbertsen, A., Geng, Z., Johnson, C., Young, B., Henke, C., et al. (2017). Lactate promotes synthetic phenotype in vascular smooth muscle cells. *Circ. Res.* 121, 1251–1262.

Yin, L.M., and Xu, Y.D. (2018). Transgelin-2 as a therapeutic target for asthmatic pulmonary resistance. *Sci. Transl. Med.* 10, eaam8604.

Zeng, M., Luo, Y., Xu, C., Li, R., Chen, N., Deng, X., Fang, D., Wang, L., Wu, J., and Luo, M. (2019). Platelet-endothelial cell interactions modulate smooth muscle cell phenotype in an in vitro model of type 2 diabetes mellitus. *Am. J. Physiol. Cell Physiol.* 316, C186–c197.

Zhang, M.J., Sun, J.J., Qian, L., Liu, Z., Zhang, Z., Cao, W., Li, W., and Xu, Y. (2011). Human umbilical mesenchymal stem cells enhance the expression of neurotrophic factors and protect ataxic mice. *Brain Res.* 1402, 122–131.

Zhang, X., Zhu, X.L., Ji, B.Y., Cao, X., Yu, L.J., Zhang, Y., Bao, X.Y., and Xu, Y. (2019). LncRNA-1810034E14Rik reduces microglia activation in experimental ischemic stroke. *J. Inflamm.* 16, 75.

Zhao, Z., Nelson, A.R., Betsholtz, C., and Zlokovic, B.V. (2015). Establishment and dysfunction of the blood-brain barrier. *Cell* 163, 1064–1078.

Zheng, J., Dai, Q., Han, K., Hong, W., Jia, D., Mo, Y., Lv, Y., Tang, H., Fu, H., and Geng, W. (2020). JNK-IN-8, a c-Jun N-terminal kinase inhibitor, improves functional recovery through suppressing neuroinflammation in ischemic stroke. *J. Cell Physiol.* 235, 2792–2799.

Zhou, Y., Liu, X., Huang, N., and Chen, Y. (2019). Magnesium ion leachables induce a conversion of contractile vascular smooth muscle cells to an inflammatory phenotype. *J. Biomed. Mater. Res. B Appl. Biomater* 107, 988–1001.

STAR★ METHODS

KEY RESOURCES TABLE

REAGENT or RESOURCE	SOURCE	IDENTIFIER
Antibodies		
Rabbit monoclonal anti-MYPT1	Cell Signaling Technology	Cat#2634; RRID: AB_915965
Rabbit polyclonal anti-ZO-1	Thermo Fisher Scientific	Cat#402-2200; RRID: AB_2533456
Mouse monoclonal anti-Occludin	Thermo Fisher Scientific	Cat#33-1500; RRID: AB_2533101
Rabbit polyclonal anti-Claudin 5	Abcam	Cat#ab15106; RRID: AB_301652
Mouse monoclonal anti- α -SMA	R&D Systems	Cat#MAB1420; RRID: AB_262054
Rabbit monoclonal anti-Calponin	Abcam	Cat#ab46794; RRID: AB_2291941
Rabbit polyclonal anti-SM22 α	Abcam	Cat#ab14106; RRID: AB_443021
Rabbit polyclonal anti-ECSIT	Abcam	Cat#ab21288; RRID: AB_446163
Rabbit polyclonal anti-GAPDH	Bioworld Technology	Cat#AP0063; RRID: AB_2651132
Mouse monoclonal anti-Tubulin- α	Santa Cruz Biotechnology	Cat#sc-398103; RRID: AB_2832217
Mouse monoclonal anti-CD31	Abcam	Cat#ab24590; RRID: AB_448167
Rat monoclonal anti-CD31	Santa Cruz Biotechnology	Cat#sc-18916; RRID: AB_627028
Rabbit polyclonal anti VE-cadherin	Abcam	Cat#ab33168; RRID: AB_870662
Chemicals, peptides, and recombinant proteins		
Evans blue	Sigma	Cat#E2129
FITC-dextran	Sigma	Cat#46945
Recombinant Human IL-6 Protein	R&D Systems	Cat#206-IL
Tocilizumab	Topscience	Cat#T9911
Critical commercial assays		
PrimeScript RT reagent Kit	Takara	Cat #RR037A
SYBR green Kit	Takara	Cat #DRR820A
CBA Human Inflammation Kit	BD Biosciences	Cat #551811
Deposited data		
Raw LC-MS/MS data	This paper	ProteomeXchange Consortium, PRIDE: PXD0027869
Experimental models: Cell lines		
Human brain vascular smooth muscle cells	ScienCell Research Laboratories	Cat#1100
Human brain microvascular endothelial cells	ScienCell Research Laboratories	Cat#1000
Experimental models: Organisms/strains		
MYPT1 ^{SMKO} mice	(He et al., 2013)	N/A
Software and algorithms		
ImageJ software	NIH	https://imagej.nih.gov/ij/
FCAP Array software	Soft Flow Hungary Ltd	http://softflow.com
GraphPad Prism 7 software	Graphpad	http://www.graphpad.com

RESOURCE AVAILABILITY

Lead contact

Further information and requests for resources and reagents should be directed and will be fulfilled by the Lead Contact, Yun Xu (xuyun20042001@aliyun.com).

Materials availability

This study did not generate new unique reagents.

Data and code availability

The mass spectrometry proteomics data have been deposited to the ProteomeXchange Consortium via the PRIDE (Perez-Riverol et al., 2019) partner repository with the dataset identifier PXD027869. All original code is publicly available as of the date of publication. DOIs are listed in the key resources table. Any additional information required to reanalyze the data reported in this paper is available from the lead contact upon request.

EXPERIMENTAL MODEL AND SUBJECT DETAILS

Animals

Mice were maintained in specific pathogen-free animal facilities at the Affiliated Drum Tower Hospital of Nanjing University Medical School. All animal experiments were performed in accordance with institutional guidelines and approved by the Animal Care Committee of Nanjing University. MYPT1^{fl_{ox}/fl_{ox}} mice were provided from the Model Animal Research Center of Nanjing University. In brief, the CreloxP system were used to establish Mypt1-floxed mice, with the promoter region and exon 1 of Mypt1 flanked by 2 loxP sites. These mice were crossed with SMA-Cre transgenic mice to generate mice with smooth muscle-specific deletion of MYPT1 (MYPT1^{SMKO} mice) (He et al., 2013). The littermates of MYPT1^{fl_{ox}/+} SMA-Cre mice were used as controls. Genotypes were determined by PCR. Male mice between 12-14 weeks of age weighing 22-24 g were used indiscriminately.

METHOD DETAILS

Ischemia model in mice

Male mice between 12-14 weeks of age weighing 22-24 g were subjected to middle cerebral artery occlusion (MCAO) by the intraluminal filament technique. After anesthesia, 6/0 sutures (Doccol Corporation, MA, USA) were inserted into the middle cerebral artery until the ipsilateral blood flow decreased to below 30% of baseline, as monitored by a laser Doppler flowmetry (Perimed Corporation, Stockholm, Sweden). The ipsilateral blood flow of the mice was restored after 60 min. The sham mice underwent the same operation except insertion of the filament into the middle cerebral artery.

Behavior tests

Neurological behavior tests, including the modified neurological severity score (mNSS) test, rotarod test, foot fault test and forelimb grip strength test, were used to evaluate the neurological function of the mice from day 1 to day 7 after MCAO. The mNSS test is a composite test of sensory function, motor function, reflexes and balance. Scores from 1 to 12, with a higher score indicating more severe disease (Chen et al., 2001). The rotarod test (IITC Life Science, USA) was used to assess motor deficits and sensorimotor coordination in the MCAO mice. The mice were subjected to 3-day training sessions, during which they ran at speeds of 10, 20, 30 and 40 rpm for 5 min at an interval of 30 min. The time that the mice spent on the rod at a speed of 40 rpm was recorded from day 0 to day 7 after MCAO (Zhang et al., 2011). The foot fault test is a tool for assessing locomotor and sensory function (Zheng et al., 2020). The error rate was calculated as the number of times the left forelimb slipped off relative to the total number of steps. The forelimb grip strength test was performed with a grip strength meter (BIOSEB, USA). The paws of each mouse were placed on a metal T-bar, the mouse was habituated to hold onto the bar, and the tail was gently pulled backwards. The maximum strength of the grip prior to release was recorded (Alamri et al., 2018). All neurological behavior tests were performed by an investigator who was blinded to the experimental groups.

Infarct volume calculation

To evaluate the infarct size of brain tissue, 2% 2,3,5-triphenyltetrazolium chloride (TTC; Sigma-Aldrich) staining was used. The brains were quickly removed after the mice were anesthetized and cut into six 1-mm-thick coronal slices, which were then stained with TTC for 20 min at 37°C (Wu et al., 2019a). Images were taken with a digital camera and analyzed by ImageJ software (National Institutes of Health). The infarct volume was calculated as a percentage of the volume of the bilateral side.

Quantitation of BBB permeability

The Evans blue (EB) extravasation assay was performed to assess BBB permeability. Mice were injected with EB (2% in 0.9% saline; 3 ml/kg, Sigma-Aldrich) via the tail vein. Two hours later, the mice were perfused with 0.9% saline under deep anesthesia, and then the brains were cut into slices for analysis. Each hemisphere was weighed and homogenized in N, N-dimethyl formamide (Sigma-Aldrich). The samples were centrifuged and collected. The EB concentration in the supernatant was determined with a microplate reader (Tecan Trading, AG, Switzerland) at 620 nm. The amount of EB extravasated from each sample was expressed as micrograms per gram of wet tissue (Sun et al., 2017).

FITC-dextran (70 kDa, Sigma, #46945) was employed to evaluate the change in BBB integrity. Mice were injected with FITC-dextran (1 mg/kg body weight) in 0.9% saline after anesthesia. After 30 min, the brains were collected and frozen at -80 °C for 2 h. Then, the brains were cut into 30 μm slices with a freezing microtome (Leica) and visualized directly under a fluorescence microscope. The FITC-dextran leakage area was determined with ImageJ software (National Institutes of Health).

Electron microscope

Cortical vessels were collected from the ipsilateral and contralateral hemispheres. Approximately 2 mm³ cubes of representative vessels were obtained and fixed in 2.5% glutaraldehyde (Servicebio) for 2-4 h. After being washed with PBS 3 times, the vessels were fixed in 1% osmium tetroxide for 2 h, dehydrated and embedded in 812 embedding medium (SPI). Ultrathin sections were cut with a diamond cutter (Daitome). Lead citrate and uranyl acetate contrasted ultrathin sections were examined using an electron microscope (HITACHI).

Cortical small vessel preparation

The brains were quickly removed after the mice were anesthetized and placed in ice-cold PBS at 4 °C. The cortical arterioles in the right hemisphere were removed by dissecting forceps carefully separate the blood vessel segments containing MCA branches, LMA and ACA branches in the pia mater under a microscope, and placed into a 1.5 ml EP tube containing 200 μl ice-cold PBS. The vessels were centrifuged at 1000 rpm for 5 min at 4 °C. The supernatant was removed and the vessels were collected for the next step.

Western blotting analysis

Cortical arterioles were lysed with RIPA lysis buffer (Thermo Fisher, #89901) and protease inhibitor (Thermo Fisher, #87785). BCA (Thermo Fisher, #A53226) was used to measure the protein concentration. After the proteins were prepared and loaded into gels, they were electrophoresed, transferred to PVDF membranes, and blocked with 5% milk in tris-buffered saline with Tween 20. The blots were then probed with antibodies against MYPT1 (1:1000, CST, #2634), ZO-1 (1:1000, Invitrogen, #402-2200), Occludin (1:1000, Invitrogen, #33-1500), Claudin 5 (1:1000, Abcam, #ab15106), α-SMA (1:1000, R&D, MAB1420), Calponin (1:1000, Abcam, #ab46794), SM22α (1:1000, Abcam, #ab14106), ECSIT (1:1000, Abcam, #ab21288), glyceraldehyde-3-phosphate dehydrogenase (GAPDH) (1:1000, Bioworld, #AP0063), and Tubulin-α (1:1000, Santa Cruz Biotechnology, sc-398103) and then incubated with horseradish peroxidase (HRP)-conjugated anti-rabbit (1:2000, CST) and anti-mouse (1:2000, CST). The blots were developed using enhanced chemiluminescence (Life Technologies) and quantified with ImageJ software.

RNA isolation and quantitative real-time PCR

Cortical arterioles and cell samples were lysed with TRIzol reagent (Invitrogen). Total RNA was isolated according to the standard protocol provided by Invitrogen and the quality of the RNA was assessed with a Nanodrop 2100 spectrophotometer (Agilent). Then, the RNA was reverse-transcribed into cDNA with a PrimeScript RT reagent Kit (Takara, #RR037A). Quantitative real-time PCR was performed on an ABI 7500 PCR instrument (Applied Biosystems) with a SYBR green Kit (Takara, #DRR820A). The mRNA expression in each sample was calculated by the 2^{-(ΔΔCt)} method after normalization to the expression of the internal control GAPDH. The primer sequences are shown in the Table S1.

Immunofluorescence staining

The mice were perfused with 0.9% saline and 4% paraformaldehyde after deep anesthesia. After being soaked in 4% paraformaldehyde for 24 h, the brains were dehydrated in 15% and 30% glucose solutions for 24 h (Zhang et al., 2019). After being drying, the brains were frozen at -80°C for at least 48 h and

then cut into 20 μm slices with a freezing microtome (Leica). The brain slices were incubated at 4°C overnight with 2% bovine serum albumin, comprising CD31 (1:200, Abcam, #ab24590), ZO-1 (1:1000, Invitrogen, #402-2200), Occludin (1:1000, Invitrogen, #33-1500), Claudin 5 (1:1000, Abcam, #ab15106), α -SMA (1:1000, R&D, #A5228), SM22 α (1:1000, Abcam, #ab14106) and VE-cadherin (1:500, Abcam, #ab33168). The slices were incubated with donkey anti-rabbit, donkey anti-mouse and donkey anti-rat secondary antibodies (1:500, Invitrogen) at room temperature for 2 h after being washed 3 times with PBS. A DAPI staining kit (1:1000, Bioworld) was used to label the nuclei. The slices were then photographed with a fluorescence microscope (Olympus) and confocal microscope (Olympus).

Proteomic analysis

Proteins of cortical arterioles were prepared immediately after cortical vessel collection (Dongsheng et al., 2016). After trypsin digestion, the peptides were desalted with a Strata X C18 SPE column (Phenomenex) and vacuum-dried. The peptides were reconstituted in 0.5 M TEAB and processed according to the protocol of the TMT kit/iTRAQ kit (Thermo Fisher). The tryptic peptides were fractionated by high pH reverse-phase HPLC using a Thermo Betasil C18 column (5 μm particles, 10 mm ID, 250 mm long). The peptides were subjected to a nanospray ionization (NSI) source followed by tandem mass spectrometry (MS/MS) with a Q ExactiveTM Plus mass spectrophotometer (Thermo) coupled online to the UPLC. The resulting MS/MS data were processed using the MaxQuant search engine (v.1.5.2.8). Furthermore, bioinformatics analysis of overlapping differentially expressed proteins (DEPs) was conducted with InterProScan, the KEGG database and the STRING database version 10.1. Selected DEPs were validated by Q-PCR and Western blotting.

Cytometric bead array

The supernatant was collected from treated VSMCs, and the levels of inflammatory cytokines, including IL-8, IL-1 β , IL-6, IL-10, TNF- α and IL-12p70, were measured with a CBA Human Inflammation Kit (BD Biosciences, #551811). Cytokine standards were prepared according to the manufacturer's instructions. Each supernatant sample was mixed with 6 cytokine beads and incubated with PE detection reagent at room temperature for 3 h away from light. The beads were washed with wash buffer and centrifuged at 200 \times g for 5 min. After the beads were resuspended in wash buffer, flow cytometry was performed on an Accuri C6 flow cytometer (BD Biosciences), and the data were analyzed with FCAP Array software (Soft Flow Hungary Ltd.).

Cell cultures

Human brain vascular smooth muscle cells (HBVSMCs) were purchased from ScienCell Research Laboratories. The smooth muscle cell medium was composed of 50 ml basal medium, 1 ml fetal bovine serum, 500 μl smooth muscle cell growth supplement and 500 μl penicillin/streptomycin solution (ScienCell Research Laboratories). Human brain microvascular endothelial cells (HBMECs) were purchased from ScienCell Research Laboratories. They were cultured in ECM and RPMI 1640 (HyClone).

Ischemic model in vitro

HBVSMCs and HBMECs were seeded in 24- or 6-well plates, respectively, and subjected to oxygen-glucose deprivation/reoxygenation (OGD/R) to mimic ischemic injury. When monolayer cells covered the entire plate, the culture medium was replaced with glucose-free DMEM. Then, the cells were placed in a hypoxic chamber (Billups-Rothenberg) containing 95% N₂ and 5% CO₂. After HBVSMCs were cultured for 6 h or HBMECs were cultured for 4 h, the culture supernatant was collected, and the cells were cultured with normal medium for another 24 h. Control cells were cultured in normal medium and a normoxic environment at all times.

Lentivirus transfection

A lentivirus inhibiting MYPT1 (Lv-shMYPT1) and a control lentivirus were purchased from GeneChem (Shanghai, China). HBVSMCs were cultured and incubated with Lv-shMYPT1 (MOI=50) for 24 h and the medium was changed, and then the cells were cultured for another 72 h. HBVSMCs transfected with Lv-shMYPT1 were screened with puromycin to acquire stably transfected cells.

RNA interference

Small interfering RNAs (siRNAs) targeting human ECSIT were used to silence ECSIT in HBVSMCs transfected with Lv-shMYPT1. siRNA (100 μ mol/L) and Lipofectamine RNAiMAX Transfection Reagent (Invitrogen) were mixed and incubated at room temperature for 15 min. The mixture was added to HBVSMCs, and the cells were incubated for 24 h. The sequences of the human ECSIT-targeting siRNAs (designed and synthesized by RIBOBIO) were 5'-CAG GAA CCT CCA TCT CTC A-3', 5'-GAG GAG TGG AAC CTC TAC T-3' and 5'-GTT CCT TTG CCC AAA GAC T-3'.

Measurement of TEER

HBMECs were seeded in the upper chamber of Transwell plate. The transendothelial electrical resistance (TEER) of the HBMEC monolayer was determined with a portable epithelial volttohmmeter (EVOM, World Precision Instruments). In brief, the 4- μ m Transwell inserts containing monolayer HBMECs were placed in the 24-well plates. An EndOhm cap with two metal caps was then inserted into the medium. The short metal cap was placed in the upper chamber, and the long metal cap was placed in the lower chamber. The resistance was then measured using an EVOM resistance reader. A Transwell insert containing an equal volume of medium without HBMECs served as a blank control. All experiments were performed independently in triplicate.

FITC-dextran permeability assay

HBMECs were seeded in the upper chamber of a Transwell plate. HBMECs were treated with or without the supernatant of OGD-treated HBVSMCs for 24 h. FITC-dextran (0.1 mg/ml, 70 kDa, Sigma) was added to the HBMECs in the upper chamber. After incubation for another 20 min, 100 μ l of supernatant from the lower chamber was analyzed with a microplate reader (excitation 490 nm, emission 520 nm). There were at least 6 wells per group, and 3 independent experiments were performed.

IL-6 and tocilizumab application

HBMECs were stimulated with 20 ng/ml recombinant human IL-6 protein (R&D) for 1 d. Then HBMEC permeability was evaluated by Western blotting, FITC-dextran labeling and TEER measurement.

Tocilizumab (Topsience) is a humanized monoclonal antibody that specifically inhibits the binding of IL-6 to its receptor. The supernatant of MYPT1-deficient HBVSMCs treated with OGD was administered to HBMECs treated with or without OGD. In the IL-6 inhibition experiment, HBMECs were treated with excess tocilizumab (5 μ g/ml) for 48 h in parallel. In vivo, 5 mg/kg/d tocilizumab was injected intraperitoneally into MYPT1^{SMKO} mice for 1 d after MCAO (Shinriki et al., 2009). An equal volume of PBS was used as control.

QUANTIFICATION AND STATISTICAL ANALYSIS

SPSS 15.0 software was used for analysis of the experimental data. One-way ANOVA followed by Bonferroni's post hoc test was used when only one factor was involved, and two-way ANOVA followed by Tukey's test for multiple comparisons was used when two factors were involved. Additionally, Student's t test was used to compare the differences between two groups. The data are expressed as the mean \pm SEM. $P < 0.05$ was considered significant. GraphPad Prism 7 software was used to make graphs.